PAPER

Highly asymmetric probability distribution from a finite-width upward step during inflation

To cite this article: Ryodai Kawaguchi *et al* JCAP11(2023)021

View the article online for updates and enhancements.

JCAP ANNIVERSARY SPECIAL ISSUE

Highly asymmetric probability distribution from a finite-width upward step during inflation

Ryodai Kawaguchi,[a] **Tomohiro Fujita**[b,c] **and Misao Sasaki**[d,e,f]

[a]*Department of Physics, Waseda University,*
3-4-1 Okubo, Shinjuku, Tokyo 169-8555, Japan
[b]*Waseda Institute for Advanced Study, Waseda University,*
1-6-1 Nishi-Waseda, Shinjuku, Tokyo 169-8050, Japan
[c]*Research Center for the Early Universe, The University of Tokyo,*
Bunkyo, Tokyo 113-0033, Japan
[d]*Kavli Institute for the Physics and Mathematics of the Universe (WPI),*
The University of Tokyo Institutes for Advanced Study, The University of Tokyo,
Chiba 277-8583, Japan
[e]*Center for Gravitational Physics and Quantum Information,*
Yukawa Institute for Theoretical Physics, Kyoto University,
Kyoto 606-8502, Japan
[f]*Leung Center for Cosmology and Particle Astrophysics, National Taiwan University,*
Taipei 10617, Taiwan

E-mail: ryodai0602@fuji.waseda.jp, zitenkan1@gmail.com, misao@yukawa.kyoto-u.ac.jp

ABSTRACT: We study a single-field inflation model in which the inflaton potential has an upward step between two slow-roll regimes by taking into account the finite width of the step. We calculate the probability distribution function (PDF) of the curvature perturbation $P[\mathcal{R}]$ using the δN formalism. The PDF has an exponential-tail only for positive $\mathcal{R}$ whose slope depends on the step width. We find that the tail may have a significant impact on the estimation of the primordial black hole abundance. We also show that the PDF $P[\mathcal{R}]$ becomes highly asymmetric on a particular scale exiting the horizon before the step, at which the curvature power spectrum has a dip. This asymmetric PDF may leave an interesting signature in the large scale structure such as voids.

Contents

1 Introduction

The inflation theory [1–6], originally introduced to resolve the problems of the Big Bang cosmology, is currently accepted as a part of the standard cosmological model. In particular, slow-roll (SR) inflation driven by a single scalar field produces primordial fluctuations, which are nearly scale-invariant and almost Gaussian, consistent with the observed cosmic microwave background (CMB) temperature anisotropies [7, 8]. Hence, single field SR inflation is considered to be a strong candidate as an inflation model. However, the specific mechanism causing inflation is still unknown, and various inflation models have been proposed within the framework of SR inflation (e.g. [1, 9–12]). Even among the canonical single scalar field models, diverse types of inflaton potentials have been studied so far. Especially at smaller scales than the CMB scale ($k \sim 0.002 \text{Mpc}^{-1}$), there are only a little observational constraints and many possible inflation scenarios are allowed.

Inflationary models associated with primordial black holes (PBHs) [13–16] have been intensively studied in recent years (e.g. ultra-slow-roll (USR) models [17–21]). PBHs are black holes formed through the gravitational collapse of regions of high density fluctuations above a threshold in the early universe. They are hypothetical objects but can play many different roles in the history of the Universe depending on their mass (see [22–31] for recent reviews). The density fluctuations originate in the curvature perturbation $\mathcal{R}$ generated during inflation, and the probability of the realisations of large curvature perturbation must be amplified by some mechanism for a sufficient abundance of PBH to be formed. The simplest way to achieve this is to enhance the power spectrum (i.e. the variance) of the curvature perturbation on a scale small compared to the CMB scale.

In general, however, the power spectrum alone does not completely fix how likely the production of large amplitude curvature perturbations is. The probabilistic characteristics of the random variable are determined solely by the power spectrum only when it follows a Gaussian distribution. In discussing deviations from Gaussian distribution in the context of primordial cosmology, higher-order correlators are often used. In particular, the non-gaussian parameter $f_{\rm NL}$ associated with the bispectrum has been discussed extensively [32–37]. While SR inflation produces almost Gaussian curvature perturbations characterized by $f_{\rm NL} \ll 1$, the inflation models in which the SR condition is violated can produce relatively large $f_{\rm NL}$ (see e.g. [38–42]). It has been pointed out that the PBH abundance is very sensitive to non-gaussianity in such cases (e.g. [43–58]).

The large and rare fluctuations that cause PBH formation cannot be precisely assessed by perturbative methods alone such as the $f_{\rm NL}$ parameter. To capture their nature, we can use a powerful non-perturbative approach called the δN formalism [59–66]. This formalism allows a direct conversion from the probability distribution function (PDF) of the scalar field perturbation $\delta\varphi$ to the PDF of $\mathcal{R}$. It is known that in inflationary models leading to PBH formation, an exponential tail appears in the PDF of $\mathcal{R}$, which has a significant impact on the PBH abundance [67–73] (see also stochastic approach [74–79]).

This paper focuses on a model where the inflaton potential has an upward step between two SR regions [80–82]. Models with such an abrupt change have been studied extensively (e.g. [67, 80–92]) and tend to be consistent with the CMB observations, as the transition takes less time and does not affect much the SR inflaton dynamics on the CMB scale. Previous studies of the upward step model calculated the PDF of $\mathcal{R}$ by ignoring the finite width of the step and reported that the PDF has a hard cutoff at a certain value of $\mathcal{R}$ beyond which the PDF is zero [81, 82]. In this paper, we take a step width $\Delta\varphi$ into consideration. We introduce a smooth step whose first-order derivative is continuous, and investigate the probabilistic features of the curvature perturbation using the classical δN formalism. We also discuss the impact of the finite step width on the PBH abundance.[1]

We obtain two main results. The first reveals that a tail dependent on the step width $\Delta\varphi$ appears in the PDF, and the cutoff feature disappears. In the zero-width limit $\Delta\varphi \to 0$, the

---

[1]Recently, there are active debates if the enhancement of the curvature power spectrum on the small scale for PBH generation could significantly affect the power spectrum on the CMB scale due to the one-loop correction, since ref. [93] raised this issue (see also [94]). There are some counter arguments and this is still unsettled issue [95–106]. In particular, it is advocated that the loop correction can be sufficiently suppressed by considering smooth transition between SR and USR [100–102]. We do not address this issue in the present paper, but it gives another motivation for introducing the step width $\Delta\varphi$ that smooths the transition.

tail becomes steeper and eventually the cutoff is reproduced. The complementary cumulative distribution function is then calculated, showing that the step width $\Delta\varphi$ has a significant impact on the estimate of PBH abundance. The second is the discovery of a PDF with very high asymmetry. At certain scales exiting the Hubble horizon before the step, $\mathcal{R}$ cannot take large negative values and the PDF becomes asymmetric. The scale that is most asymmetric is shown to correspond to the dip scale, where $\langle(\mathcal{R}-\langle\mathcal{R}\rangle)^2\rangle$ and $\langle(\mathcal{R}-\langle\mathcal{R}\rangle)^3\rangle$ are the smallest compared to the other scales. By illustrating the spatial distribution realized with the highly asymmetric PDF, we show that the fraction of low-density regions is smaller at the dip scale.

This paper is organized as follows. In section 2, we explain the details of our model in which the inflaton potential includes an upward step between two SR regions. In section 3, the background equation of motion is solved, and in section 4 we derive the relation between the curvature perturbation $\mathcal{R}$ and the scalar perturbation $\delta\varphi$ using the δN formalism. In section 5, we compute the PDF and the CCDF of $\mathcal{R}$ and show that the exponential tail, which depends on $\Delta\varphi$, appears. In section 6 we show that the highly asymmetric PDF appears and relate it to the dip scale. We then briefly discuss the implications of the highly asymmetric PDF for the structure of the universe. Section 7 is devoted to conclusions.

2 Upward-step model

In this section, we describe the setup of our model. Let us consider a single-field inflationary model with a scalar field ϕ,

$$\mathcal{S} = \int \mathrm{d}^4x \sqrt{-g}\left[\frac{M_{\mathrm{pl}}^2}{2}R - \frac{1}{2}g^{\mu\nu}\partial_\mu\phi\partial_\nu\phi - V(\phi)\right], \tag{2.1}$$

where g is a determinant of the metric tensor $g_{\mu\nu}$ and $V(\phi)$ is a potential of the scalar field. We consider a spatially flat Friedmann-Lemaître-Robertson-Walker background, $\mathrm{d}s^2 = -\mathrm{d}t^2 + a^2(t)\delta_{ij}\mathrm{d}x^i\mathrm{d}x^j$, where $a(t)$ is a time-dependent scale factor. From the above action, we obtain two background equations of motion

$$3h^2 = \frac{1}{2}h^2\pi^2 + v\,, \tag{2.2}$$

$$\frac{\mathrm{d}\pi}{\mathrm{d}n} + \frac{v}{h^2}\pi + \frac{\partial_\varphi v}{h^2} = 0\,, \tag{2.3}$$

where we introduced dimensionless quantities, $\varphi \equiv \phi/M_{\mathrm{pl}}$, $\pi \equiv \mathrm{d}\varphi/\mathrm{d}n$, $v \equiv V(\phi)/V_0$ and $h \equiv M_{\mathrm{pl}}H/\sqrt{V_0}$. V_0 is an arbitrary reference point of the potential, $H = \dot{a}/a$ is the Hubble expansion rate and n is the number of e-folds defined by $\mathrm{d}n = H\mathrm{d}t$. Without loss of generality, we assume that φ moves from positive to zero along the potential and π is always negative during inflation.

In our model, the potential $v(\varphi)$ has an upward step-like feature between two slow-roll regions,

$$v(\varphi) = \begin{cases} v_{\mathrm{sr1}}(\varphi) & (\varphi \geq \varphi_1) \\ f_{\mathrm{step}}(\varphi) & (\varphi_2 < \varphi < \varphi_1)\,, \\ v_{\mathrm{sr2}}(\varphi) & (\varphi \leq \varphi_2) \end{cases} \tag{2.4}$$
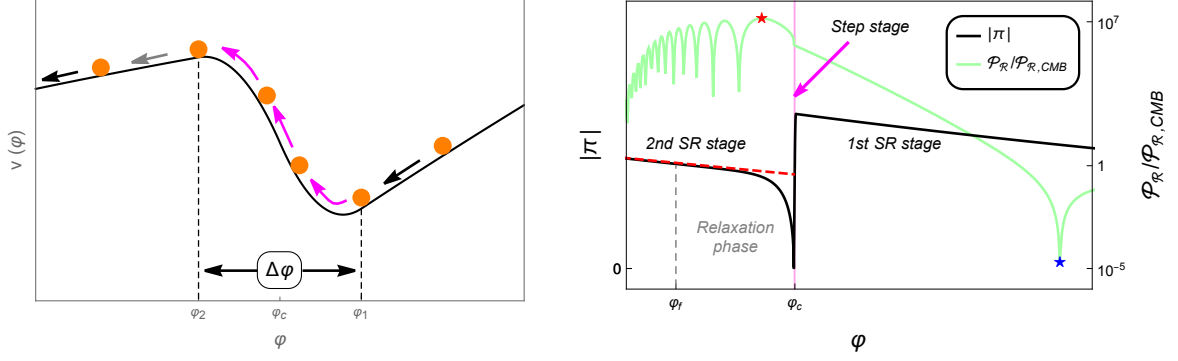
Figure 1. (Left panel) Schematic figure of the potential (black solid line) and the scalar field (orange balls). Two slow-roll (SR) potentials are connected by a smooth upward step with the width $\Delta\varphi$. The black, magenta and gray arrows represent the SR, step-climbing and relaxation phases, respectively. (Right panel) Schematic figure of the background trajectory in the phase space. The scalar field evolves from right to left in time, and experiences (i) the first SR stage, (ii) the step stage highlighted by magenta shading, and (iii) the second SR stage. At the beginning of the second SR stage, the trajectory deviates from the SR attractor (red dashed line), which is called the relaxation phase. For reference, we superimposed the shape of the linear order power spectrum on the right panel and indicated the positions of its peak and dip (red and blue stars).

where $v_{\rm sr1}$ and $v_{\rm sr2}$ are slow-roll (SR) potentials, which are generally different from each other and satisfy $v_{\rm sr2}(\varphi_2) > v_{\rm sr1}(\varphi_1)$ to have an upward step in between. The width of the step region will be an important parameter

$$\Delta\varphi \equiv \varphi_1 - \varphi_2. \tag{2.5}$$

For the upward step $f_{\rm step}$, we employ quadratic functions

$$f_{\rm step}(\varphi) = \begin{cases} A_1 + B_1(\varphi - \varphi_{\rm min})^2 & (\varphi_c \leq \varphi < \varphi_1 : \text{ S1 region}) \\ A_2 + B_2(\varphi - \varphi_{\rm max})^2 & (\varphi_2 < \varphi < \varphi_c : \text{ S2 region}) \end{cases}, \tag{2.6}$$

where $\varphi_c \equiv (\varphi_1 + \varphi_2)/2$ is the midpoint of the step region. $\varphi_{\rm min}$ and $\varphi_{\rm max}$ denote the minimum and maximum of the quadratic potential, respectively. Requiring that the potential and its first φ-derivative are continuous at $\varphi = \varphi_c, \varphi_1$, and φ_2, the six constants $A_1, A_2, B_1, B_2, \varphi_{\rm min}, \varphi_{\rm max}$ are thereby determined as shown in appendix A.

The left panel of figure 1 schematically shows our potential $v(\varphi)$. We chose $v_{\rm sr1}$ and $v_{\rm sr2}$ so that their slopes are different before and after the upward step, for example, $\partial_\varphi v_{\rm sr1}(\varphi_1) > \partial_\varphi v_{\rm sr2}(\varphi_2)$. The right panel of figure 1 schematically shows the background trajectory in the phase space. Due to the presence of the upward step, there are three distinct stages of the background evolution: (i) The first stage, $\varphi \geq \varphi_1$, is the first SR stage where the background trajectory is on the SR attractor. (ii) The second, $\varphi_2 < \varphi < \varphi_1$, is the step stage. In the step stage, the scalar field rapidly loses its kinetic energy and $|\pi|$ becomes smaller than before the step. (iii) The third, $\varphi \leq \varphi_2$, is the second SR stage. Since $|\pi|$ is made smaller by the step, the trajectory in the phase space is not on the SR attractor right after the scalar field finishes climbing up the step. Therefore, after the step, a relaxation phase takes place and the scalar

field asymptotically approaches to the second SR attractor. Eventually, the trajectory can be regarded as settling on the SR attractor, and we call the scalar field value at that time as φ_f.

For later convenience, we conclude this section by defining useful quantities as follows.

$$\eta_i \equiv 2(2\epsilon_{Vi} - \eta_{Vi}), \tag{2.7}$$

$$g \equiv \frac{\pi_2}{\pi_1} < 1, \tag{2.8}$$

$$\kappa \equiv \sqrt{\frac{\epsilon_{V1}}{\epsilon_{V2}}}, \tag{2.9}$$

$$\omega_{s1} \equiv \sqrt{\frac{6B_1}{A_1}} \simeq \frac{\sqrt{2}\,|\pi_1|}{\Delta\varphi}, \tag{2.10}$$

$$\omega_{s2} \equiv \sqrt{\frac{-6B_2}{A_2}} \simeq \frac{\sqrt{2}\,|\pi_1|}{\Delta\varphi}, \tag{2.11}$$

where $\epsilon_V \equiv (\partial_\varphi v/v)^2/2$ and $\eta_V \equiv \partial_{\varphi\varphi} v/v$ are the potential slow-roll parameters and the subscript i indicates that a quantity is evaluated at $\varphi = \varphi_i$ ($i = 1, 2$). The approximations used in eqs. (2.10) and (2.11) assume $\Delta\varphi \ll |\pi_1|$ and $g \ll 1$, and the dependence of ω_{s1} and ω_{s2} on $\Delta\varphi$ will be emphasized in the later discussion.

3 Background solution

In this section, we briefly discuss the background behavior of the scalar field in each of the three stages. In solving the background equation of motion (2.3), we use the following three approximations. (I) The kinetic energy of the scalar field is subdominant compared to the potential energy, $h^2\pi^2 \ll v$. (II) Assuming the width of the step $\Delta\varphi$ is sufficiently small, we keep only its leading contributions. Consequently, $\varphi_{\min}$ and $\varphi_{\max}$ are identified with φ_1 and φ_2, respectively. (III) The Hubble friction is negligible in the step stage. The detailed derivations of the solutions and the discussions on the limitations of the above approximations can be found in appendices B and D.

In the SR stages, a general SR solution is applicable,

$$\varphi(n) - \varphi_i = \frac{2\sqrt{2\epsilon_{Vi}}}{\eta_i}\Big(1 - e^{\frac{\eta_i}{2}(n-n_i)}\Big) + \frac{1}{3}\Big(\pi_i + \sqrt{2\epsilon_{Vi}}\Big)\Big(e^{\frac{\eta_i}{2}(n-n_i)} - e^{-(3+\frac{\eta_i}{2})(n-n_i)}\Big). \tag{3.1}$$

Again, we used the shorthand notation $X_i \equiv X(\varphi_i)$. One needs to know π_i to fix the boundary condition. In the first SR stage, the background trajectory is on the SR attractor, i.e. $\pi_1 = -\sqrt{2\epsilon_{V1}}$ and hence the second term in eq. (3.1) vanishes. In the second SR stage, however, the trajectory is not on the attractor in the relaxation phase (see figure 1). To find π_2 we use the approximated energy conservation during the step stage,

$$\pi_2 = -\sqrt{\pi_1^2 + 6\log\left(\frac{v(\varphi_1)}{v(\varphi_2)}\right)}. \tag{3.2}$$

Here $\pi^2/2 + 3\log(v)$ is conserved, because the background equation of motion with the above approximations (I) and (III) reduces to $d\pi/dn + 3\partial_\varphi \log(v) = 0$ as shown in eq. (B.1).

The step stage is split into the S1 and S2 region, which has a normal and inverted harmonic potential, respectively (see eq. (2.6)). The background solutions in these regions are

$$\varphi(n) - \varphi_1 = \frac{\pi_1}{\omega_{\text{s}1}} \sin(\omega_{\text{s}1}(n - n_1)), \qquad (\varphi_c \leq \varphi < \varphi_1) \tag{3.3}$$

$$\varphi(n) - \varphi_2 = \frac{\pi_2}{\omega_{\text{s}2}} \sinh(\omega_{\text{s}2}(n - n_2)). \qquad (\varphi_2 < \varphi < \varphi_c) \tag{3.4}$$

Note that for extremely small π_2, eq. (3.4) can be inverted as $\omega_{s2}(n_2 - n) \simeq \log(2\omega_{s2}(\varphi(n) - \varphi_2)/|\pi_2|)$. This implies that it takes logarithmically longer time for the background inflaton to climb up the upward step for smaller π_2. It will have a significant impact on the final result.

4 Calculation of δN

We now turn our attention to the curvature perturbation $\mathcal{R}$. According to the δN formalism, the curvature perturbation $\mathcal{R}$ can be calculated as the difference in the number of e-folds between the perturbed spacetime and the background spacetime [59–65],

$$\mathcal{R} = \delta N \equiv N(\varphi + \delta\varphi, \pi + \delta\pi; \varphi_f, \pi_f) - N(\varphi, \pi; \varphi_f, \pi_f), \tag{4.1}$$

where $N(\varphi, \pi; \varphi', \pi')$ is the number of e-folds for which the inflaton takes to evolve from (φ, π) to (φ', π') in the phase space. In this paper, we assign (φ, π) to the background value at the horizon crossing time for a scale of interest k. Note that the velocity perturbation $\delta\pi$ at the starting point is assumed to be negligibly small. In what follows, we start from φ on the first SR attractor ($\varphi > \varphi_1$), and compute δN generated in all stages.[2]

In the first SR stage, the initial perturbation $\delta\varphi$ induces δN as well as the velocity perturbation at the end of the first stage $\delta\pi_1$. We obtain them by comparing eq. (3.1) at $i = 1$ to its perturbed expression with $\varphi \to \varphi + \delta\varphi$ and $\pi_1 \to \pi_1 + \delta\pi_1$ as (see appendix C.1 for derivation)

$$\delta N^{(1)} \simeq -\frac{\delta\varphi}{\pi}, \qquad \delta\pi_1 \simeq -\frac{\eta_1}{2}\left(\frac{\pi}{\pi_1}\right)^{\frac{6}{\eta_1}} \delta\varphi, \tag{4.2}$$

where $\delta N^{(1)}$ denotes the contribution to total δN from the first SR stage. This approximation is valid for $|\delta N^{(1)}| \ll 1/3$. One can apparently choose φ from any values within the first SR stage. However, since $6/\eta_1$ is large, if we choose φ far from the step, $\delta\pi_1$ would be substantially suppressed by the factor $(\pi/\pi_1)^{6/\eta_1}$. This is a consequence of the fact that the background trajectory is an attractor in the first SR stage. If $\delta\pi_1$ is strongly suppressed, there would be no significant contribution to total δN from the subsequent evolution in the step stage. In this paper, therefore, we consider φ close to φ_1 and investigate the effect of the upward step on the curvature perturbations, that exit the horizon slightly before entering the step stage.

---

[2]The e-folding number taken for the inflaton to pass through the step stage is only about $\Delta N \sim 1/\omega_{\text{s}1} \ll 1$ and the corresponding band of wavenumbers that exit the Hubble horizon during the step stage, is very narrow. Thus, we do not consider curvature perturbations on such scales in this paper. The scales crossing the Hubble horizon after the step stage are not studied in this paper either, as they are similar to the normal SR case, although the evolution of $\delta\varphi$ well inside the horizon is affected by the step.

In the second SR stage, δN is produced by $\delta\pi_2$, contrary to $\delta N^{(1)}$ induced by $\delta\varphi$. Perturbing eq. (3.2), we find that $\delta\pi_2$ is given by

$$\delta\pi_2 = \pi_2\left(\sqrt{1 + \frac{2}{g^2}\frac{\delta\pi_1}{\pi_1} + \frac{1}{g^2}\left(\frac{\delta\pi_1}{\pi_1}\right)^2} - 1\right), \tag{4.3}$$

where the Hubble friction in the step stage was ignored. Using eq. (3.1) at $i = 2$ in a similar way to eq. (4.2) but only with $\pi_2 \to \pi_2 + \delta\pi_2$, we obtain the contribution to δN from the second SR stage as (see appendix C.2)

$$\delta N^{(2)} \simeq -\frac{\kappa g}{3}\frac{\delta\pi_2}{\pi_2} \simeq \frac{\kappa g}{3}\left(1 - \sqrt{1 + \frac{2}{g^2}\frac{\delta\pi_1}{\pi_1} + \frac{1}{g^2}\left(\frac{\delta\pi_1}{\pi_1}\right)^2}\right). \tag{4.4}$$

Note that the first approximate equality in eq. (4.4) relies only on $|1/\eta_2| \gg 1$ and we do not assume that $\delta\pi_2/\pi_2$ is small. Indeed, we will consider the case with $|\delta\pi_2/\pi_2| = \mathcal{O}(1)$ soon below.

The contribution to δN from the step stage is divided into two: one from the S1 region $\delta N^{(s1)}$ and the other from the S2 region $\delta N^{(s2)}$. The former is highly suppressed by $\Delta\varphi$ and $(\pi/\pi_1)^{6/\eta_1}$, and negligible compared to $\delta N^{(1)}$ (see appendix C.3). In contrast, $\delta N^{(s2)}$ can be significant. As discussed below eq. (3.4), the background e-folds of the S2 region is given by

$$N^{(s2)} \simeq \frac{1}{\omega_{s2}}\sinh^{-1}\left(\frac{\Delta\varphi}{2|\pi_2|}\omega_{s2}\right) \simeq \frac{1}{\omega_{s2}}\log\left(\frac{\Delta\varphi}{|\pi_2|}\omega_{s2}\right). \tag{4.5}$$

Perturbing it, we obtain

$$\delta N^{(s2)} \simeq -\frac{1}{\omega_{s2}}\log\left(1 + \frac{\delta\pi_2}{\pi_2}\right). \tag{4.6}$$

It is important to note that when $\delta\pi_2$ is comparable to $-\pi_2$, $\delta N^{(s2)}$ may diverge to infinity. This corresponds to the perturbed cases in which the inflaton exhausts the most of the kinetic energy to climb up the step and takes an enormous amount of time to pass through it. As we will see below, $\delta N^{(s2)}$ makes a significant impact on the curvature perturbation.

Summing up the contributions to δN from the three stages, eqs. (4.2), (4.4) and (4.6), we obtain

$$\mathcal{R} = \beta\delta\varphi + \frac{\kappa g}{3}\left(1 - \sqrt{1 + \frac{2\gamma}{g^2}\delta\varphi + \frac{\gamma^2}{g^2}\delta\varphi^2}\right) - \frac{1}{2\omega_{s2}}\log\left(1 + \frac{2\gamma}{g^2}\delta\varphi + \frac{\gamma^2}{g^2}\delta\varphi^2\right), \tag{4.7}$$

where β and γ are given by

$$\beta = -\frac{1}{\pi} > 0\,, \qquad \gamma = \frac{\eta_1\beta}{2}\left(\frac{\pi}{\pi_1}\right)^{\frac{6}{\eta_1}} \simeq \frac{\eta_1\beta}{2}\left(\frac{k}{k_1}\right)^3. \tag{4.8}$$

The second and third terms in eq. (4.7) originate from the upward step. The third term particularly comes from the finite width of the step. In fact, vanishing the step width $\Delta\varphi \to 0$ (i.e. $\omega_{s2} \to \infty$) and dropping the third term would reproduce the results of previous papers

– 7 –

that ignored the width of the step [81, 82]. Instead, substituting $g = 1$ into eq. (4.7), we obtain a similar logarithmic dependence on $\delta\varphi$ to the result in the bump-type model [67].[3]

5 Probability distribution function of $\mathcal{R}$

The second and third terms in eq. (4.7) make the curvature perturbation highly non-Gaussian. To investigate the properties of $\mathcal{R}$, we calculate its probability distribution function (PDF). The PDF of $\mathcal{R}$ is associated with the PDF of $\delta\varphi$ by probability conservation, $P[\mathcal{R}] = P[\delta\varphi]|\mathrm{d}\delta\varphi/\mathrm{d}\mathcal{R}|$. For simplicity, we assume that $\delta\varphi$ follows a Gaussian distribution with variance $\sigma_{\delta\varphi}^2$.[4] From eq. (4.7), the PDF of $\mathcal{R}$ is given by

$$P[\mathcal{R}] = \sum_i \frac{\frac{1}{\sqrt{2\pi\sigma_{\delta\varphi}^2}}\left(1 + \frac{2\gamma}{g^2}\delta\varphi_i + \frac{\gamma^2}{g^2}\delta\varphi_i^2\right)\exp\left(-\frac{\delta\varphi_i^2}{2\sigma_{\delta\varphi}^2}\right)}{\left|\beta\left(1 + \frac{2\gamma}{g^2}\delta\varphi_i + \frac{\gamma^2}{g^2}\delta\varphi_i^2\right) - \frac{\gamma}{g^2}(1 + \gamma\delta\varphi_i)\left(\frac{\kappa g}{3}\sqrt{1 + \frac{2\gamma}{g^2}\delta\varphi_i + \frac{\gamma^2}{g^2}\delta\varphi_i^2} + \frac{1}{\omega_{s2}}\right)\right|} , \quad (5.1)$$

where $\delta\varphi_i$'s ($i = a, b$) are the two solutions of eq. (4.7) for a given $\mathcal{R}$.[5] Numerically computing the above equation, we illustrate the PDF of $\mathcal{R}$ in the left panel of figure 2. One can clearly see an asymmetric non-gaussian shape of the full PDF.

To understand several features of the obtained PDF, it is useful to compare it with simplified PDFs, which take into account only one term out of three in eq. (4.7). If one term gives a dominant contribution, an analytic expression of the PDF is available. Note that for the first term, which is a linear term of $\delta\varphi$, we linearize the other terms and collect all the contributions. We find that only with the linearized, second, third term in eq. (4.7), the PDF would be (see appendix E for derivation)

$$P[\mathcal{R}] \propto \begin{cases} \exp\left[-\dfrac{\mathcal{R}^2}{2\left(\beta - \frac{\kappa\gamma}{3g} - \frac{\gamma}{\omega_{s2}g^2}\right)^2\sigma_{\delta\varphi}^2}\right] & : \text{(Gaussian)} \\[2ex] \left(1 - \dfrac{3\mathcal{R}}{g\kappa}\right)\exp\left[-\dfrac{1}{2\sigma_{\delta\varphi}^2}\dfrac{9g^2\mathcal{R}^2}{\gamma^2\kappa^2}\left(1 - \dfrac{3}{2}\dfrac{\mathcal{R}}{g\kappa}\right)^2\right] & : \text{(Cutoff)} \\[2ex] \exp(-2\omega_{s2}\mathcal{R})\exp\left[-\dfrac{1}{2\sigma_{\delta\varphi}^2}\dfrac{g^2}{4\gamma^2}\left(\exp(-2\omega_{s2}\mathcal{R}) - 1\right)^2\right] & : \text{(Exponential tail)} \end{cases} \quad (5.2)$$

where $g \ll 1$ is assumed for simplicity. We dubbed these three cases as Gaussian, Cutoff and Exponential tail after their features. The linearized term yields a Gaussian PDF. The PDF

---

[3]In the limit $g \to 1$ while keeping $\Delta\varphi$ finite, our step potential becomes a bump feature, not the featureless SR potential. The previous paper [67] computed δN only in the bump region. Hence, it is reasonable that the logarithmic term in eq. (4.7) approaches to eq. (1.5) in the previous paper [67] for $g = 1$ and $\varphi = \varphi_1$. However, its coefficient is not exactly the same but differs by $\sqrt{3}$, probably because our assumption (II) i.e. $\varphi_{\max} \simeq \varphi_2$ and $\varphi_{\min} \simeq \varphi_1$, is broken in the limit $g \to 1$.

[4]We mention that $\delta\varphi$ may have a non-Gaussianity of non-local type, arising from non-trivial higher order interactions. However, since such a non-Gaussianity is known to be perturbatively small in comparison with the local type non-Gaussianity for a canonical scalar field [107], we ignore it. Considering a possible non-perturbative effect of a non-local type non-Gaussianity is an important issue, but it is beyond the scope of the present paper.

[5]Strictly speaking there is the possibility that eq. (4.7) has another solution for a given $\mathcal{R}$ in a region $\delta\varphi < -2/\gamma$. In the following, the contribution of this solution to the probability is ignored as being small.
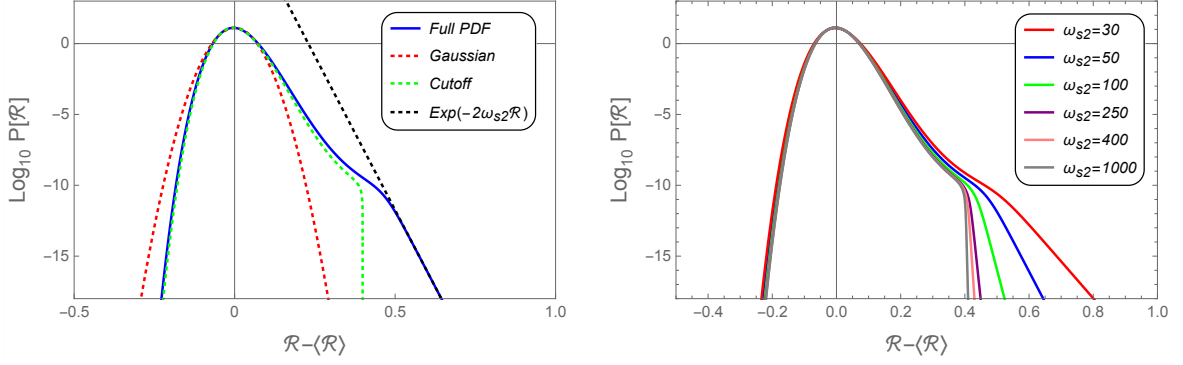
Figure 2. The probability distribution function (PDF) of the curvature perturbation $\mathcal{R}$ against $\mathcal{R} - \langle\mathcal{R}\rangle$ for $\gamma = 1.5$, $\kappa = 60$, $\beta = 20$, $g = 0.02$, and $\sigma_{\delta\varphi} = 2 \times 10^{-5}$. The mean value $\langle\mathcal{R}\rangle = \mathcal{O}(10^{-3})$ is negligibly small. (Left panel) The solid blue line denotes the full PDF obtained numerically based on eq. (5.1) for $\omega_{s2} = 50$. The coloured dotted lines represent the Gaussian (red), cutoff (green) and exponential tail (black) given in eq. (5.2). (Right panel) The coloured lines denote the full PDFs for $\omega_{s2} = 30, 50, 100, 250, 400$ and 1000 from top to bottom. They agree with the analytical behavior of the tail $P[\mathcal{R}] \propto \exp(-2\omega_{s2}\mathcal{R})$. Since $\omega_{s2} \propto 1/\Delta\varphi$, a steeper step tends to produce a steeper tail.

of the second term exhibits a sharp cutoff at $\mathcal{R} = \mathcal{R}_{\text{cutoff}} \equiv \kappa g/3$ due to its prefactor. The PDF of the third term characterized by its exponential tail, $\exp(-2\omega_{s2}\mathcal{R})$.

In the left panel of figure 2, these three simplified PDFs in eq. (5.2) are shown as dotted coloured lines in comparison with the full PDF. The full PDF (blue solid) matches the Gaussian one (red dotted) only for small $\mathcal{R} - \langle\mathcal{R}\rangle$ and their discrepancy quickly gets significant. Since we chose large $\kappa = 60$ in this figure, the second term in eq. (4.7) is dominant for a wide region, and the full and the cutoff PDF (green dotted) are well overlapped up to the cutoff position $\mathcal{R} - \langle\mathcal{R}\rangle \simeq \mathcal{R}_{\text{cutoff}} = 0.4$. For larger $\mathcal{R}$, the exponential tail from the third term (black dotted) becomes prominent, and the full PDF follows it as expected. Therefore, the cutoff feature in the PDF advocated in the previous works [81, 82] is covered up by the tail contribution as long as the finite width of the step is correctly taken into account.

To scrutinize the tail behavior, we present several PDFs with varying ω_{s2} in the right panel of figure 2. Recalling that $\omega_{s2} \propto 1/\Delta\varphi$ and the analytic tail PDF $P[\mathcal{R}] \propto \exp(-2\omega_{s2}\mathcal{R})$, we expect the slope of the tail becomes steeper as $\Delta\varphi$ decreases (i.e. the step is steeper). The figure confirms this behavior. For very large ω_{s2}, the cutoff of the PDF appears to be reproduced. However, it should be stressed that it is not a hard cutoff but a steep exponential tail. Thus, the probability density is still non-zero at $\mathcal{R} \geq \mathcal{R}_{\text{cutoff}}$ even for huge ω_{s2}.

With the evaluation of the PBH abundance in mind, we calculate the probability $\bar{F}[\mathcal{R}_c]$ where $\mathcal{R}$ is greater than or equal to the threshold value of the PBH formation $\mathcal{R}_c$, namely,

$$\bar{F}[\mathcal{R}_c] = \int_{\mathcal{R}_c}^{\infty} P[\mathcal{R}]\mathrm{d}\mathcal{R}. \tag{5.3}$$

It is called the complementary cumulative distribution function (CCDF) in the context of probability theory. We also introduce the CCDF of the Gaussian PDF

$$\bar{F}_G[\mathcal{R}_c] = \frac{1}{2}\mathrm{Erfc}\left(\frac{\mathcal{R}_c}{\sqrt{2\sigma_{\mathcal{R}}^2}}\right), \tag{5.4}$$
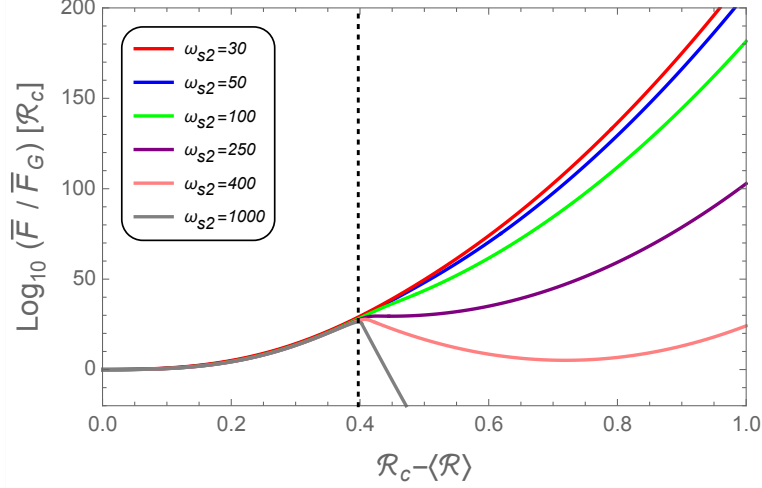
Figure 3. The complementary cumulative distribution function (CCDF) $\bar{F}[\mathcal{R}_c]$ in eq. (5.3) normalized by the Gaussian case $\bar{F}_G[\mathcal{R}_c]$ in eq. (5.4) for $\omega_{\mathrm{s}2} = 30, 50, 100, 250, 400$ and 1000 from top to bottom. The other parameters are the same as figure 2. The vertical dotted black line represents the cutoff value $\mathcal{R}_{\mathrm{cutoff}} = \kappa g/3 = 0.4$. Beyond the cutoff, the CCDF highly sensitive to $\omega_{\mathrm{s}2} \propto 1/\Delta\varphi$, because of the exponential tail contribution. Thus, the PBH abundance strongly depends on $\omega_{\mathrm{s}2}$, if $\mathcal{R}_c > \mathcal{R}_{\mathrm{cutoff}}$.

where $\mathrm{Erfc}(x)$ is the complementary error function and the variance is fixed by that of the simplified Gaussian PDF in eq. (5.2), namely $\sigma_\mathcal{R} = |\beta - \kappa\gamma/3g - \gamma/\omega_{\mathrm{s}2}g^2|\sigma_{\delta\varphi}$. Their ratio, $\bar{F}/\bar{F}_G$, is useful for understanding how much the non-Gaussianity impacts on the abundance of PBH.

In figure 3, the normalized CCDFs for different $\omega_{\mathrm{s}2}$ are shown against $\mathcal{R}_c - \langle\mathcal{R}\rangle$. The cutoff value $\mathcal{R}_{\mathrm{cutoff}}$ is also shown as a vertical black dotted line. It can be seen that the CCDF dramatically changes depending on the value of $\omega_{\mathrm{s}2}$, if $\mathcal{R}_c - \langle\mathcal{R}\rangle$ is larger than the cutoff value. For smaller $\omega_{\mathrm{s}2}$, the normalized CCDF becomes larger beyond the cutoff, because the contribution from the exponential tail is more significant in comparison to the Gaussian case. For huge $\omega_{\mathrm{s}2}$, $\bar{F}$ is abruptly suppressed at the cutoff but stays finite, because of the tail contribution. These results imply that when the critical value $\mathcal{R}_c$ of the PBH formation is larger than the cutoff $\mathcal{R}_{\mathrm{cutoff}}$, it is crucially important to take into account the finite width of the upward step for estimating the PBH abundance, because otherwise one may underestimate it.

6 Highly asymmetric PDF

In this section we will show that the PDFs with unusual shapes can be realised at certain scales exiting the Hubble horizon before the step stage and discuss its consequences. For the better understanding of this phenomenon, let us first revisit the relation between $\mathcal{R}$ and $\delta\varphi$, eq. (4.7), which has been derived in section 4.

The relation (4.7) is illustrated as a solid black line in figure 4 for $\gamma > 0$ and $\beta > \kappa\gamma/3$. In the figure, the contributions of each term in eq. (4.7) are shown as coloured dashed lines. We can see that at around $\delta\varphi = -g^2/2\gamma$, the third term (green dashed line), which is the
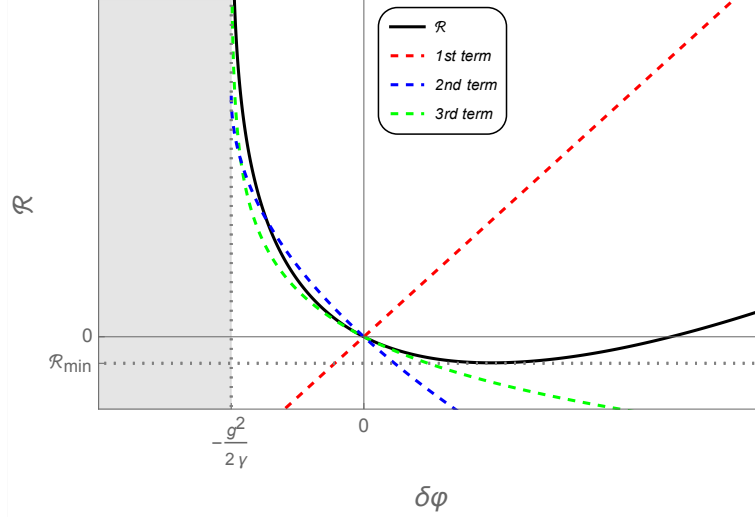
Figure 4. Schematic illustrations of eq. (4.7) for $\gamma > 0$ and $\beta > \kappa\gamma/3$. The solid black line represents the sum of the all three terms, and the dashed coloured lines represent each of them in eq. (4.7), i.e., the first term (red), the second term (blue), and the third term (green). The minimum value of $\mathcal{R}$ is denoted by the horizontal dotted line. The boundary, $-g^2/2\gamma$, is shown as the vertical dotted line. The gray shaded region corresponds to the inflaton trajectories which fail to climb the step and are stuck at a local minimum.

contribution from the step width, becomes dominant and causes $\mathcal{R}$ to diverge to infinity. This gives rise to the exponential tail in the PDF of $\mathcal{R}$.

It should be noted that there appears a local minimum of $\mathcal{R}$. For $\gamma > 0$, one can see by drawing a family of trajectories in the phase space that perturbed trajectories with $\delta\varphi < 0$ have smaller velocities $|\pi|$ at φ_1 than the background trajectory (i.e. $|\pi_1 + \delta\pi_1| < |\pi_1|$). Therefore it takes an enormous amount of time for some of the trajectories to pass through the step. As a result, they may lead to large positive δN for $\delta\varphi < 0$. One can also see that from eq. (4.7), for $\beta > \kappa\gamma/3$, the first term dominates for sufficiently large positive $\delta\varphi$, and δN increases in proportion to $\delta\varphi$. Combining the above two facts together with the fact that $\delta N = 0$ for $\delta\varphi = 0$, we can conclude that a local minimum of $\mathcal{R}$ exists, which we denote by $\mathcal{R}_{\min}$.[6] In this section, we discuss the effect of the presence of $\mathcal{R}_{\min}$ on the PDF and the local non-Gaussianity parameter $f_{\mathrm{NL}}^{\mathrm{local}}$.

Now let us take a closer look at the PDF shape and consider its consequences. Expanding eq. (4.7) with respect to $\delta\varphi$, we obtain

$$\mathcal{R} = A\delta\varphi + B\delta\varphi^2 + \mathcal{O}(\delta\varphi^3) \tag{6.1}$$

with

$$A \equiv \beta - \frac{\kappa\gamma}{3g} - \frac{\gamma}{\omega_{s2}g^2}, \qquad B \equiv \frac{\gamma^2}{g^2}\left[\frac{\kappa g}{6}\left(\frac{1}{g^2} - 1\right) + \frac{1}{2\omega_{s2}}\left(\frac{2}{g^2} - 1\right)\right]. \tag{6.2}$$

---

[6]Note that, if $\gamma < 0$, δN is a monotonically increasing function of $\delta\varphi$ and there is no $\mathcal{R}_{\min}$. Therefore, $\mathcal{R}_{\min}$ exists only if $\gamma > 0$, i.e. when the scalar field accelerates in the first SR stage.

With eq. (6.1), the local non-gaussianity parameter of $\mathcal{R}$ is defined and computed as

$$f_{\mathrm{NL}}^{\mathrm{local}} \equiv \frac{5}{3}\frac{B}{A^2} = \frac{5}{2}\frac{\kappa g(1-g^2)+\frac{3}{\omega_{\mathrm{s2}}}(2-g^2)}{\left(\frac{3\beta g^2}{\gamma}-\kappa g-\frac{3}{\omega_{\mathrm{s2}}}\right)^2}. \tag{6.3}$$

If A vanishes (i.e. $\mathcal{R}=\mathcal{R}_{\min}=0$ at $\delta\varphi=0$), the linear term in eq. (6.1) drops, the denominator of eq. (6.3) disappears, and $f_{\mathrm{NL}}^{\mathrm{local}}$ diverges.[7] It happens when $\gamma=\gamma_0 \equiv 3\beta g^2\omega_{\mathrm{s2}}/(3+\kappa g\omega_{\mathrm{s2}}) > 0$. Since γ depends on π/π_1 (see eq. (4.8)), its value varies as the scale of the curvature perturbation of interest k changes. Thus, $f_{\mathrm{NL}}^{\mathrm{local}}$ may diverge at a particular scale at which $\gamma=\gamma_0$ and $A=0$. Although diverging $f_{\mathrm{NL}}^{\mathrm{local}}$ does not mean that any physical quantity becomes singular, it is interesting to explore what kind of dynamics occurs around this particular scale.

When A vanishes, $\mathcal{R}$ can take only positive values and then the PDF only has its right-half part. This simple argument based on the expanded expression (6.1) actually applies to the fully non-linear result (4.7). In figure 5, we present the full PDF for varying γ from a larger value to $\gamma_0 = 0.3$. One can see that the full PDF deforms from a rather symmetric shape into a completely asymmetric one as the scale changes. Although it is not shown there, for $\gamma<\gamma_0$ the PDF regains its left-half part. At the lower end of the PDF of $\mathcal{R}$, many different values of $\delta\varphi$ corresponds to the minimum $\mathcal{R}$ (see figure 4), their probability density $P[\delta\varphi]$ condenses there, and $P[\mathcal{R}]$ formally diverges. However, its contribution to the total probability is negligible and harmless. In short, the peculiar behavior seen in figure 5 is not pathological, and it is remarkable to have such a highly asymmetric PDF of $\mathcal{R}$.

The most direct observables related to the PDF may be the variance and skewness of $\mathcal{R}$, i.e. $\langle(\mathcal{R}-\langle\mathcal{R}\rangle)^2\rangle$ and $\langle(\mathcal{R}-\langle\mathcal{R}\rangle)^3\rangle$. Using eq. (6.1), their ratio can be computed as

$$\frac{\langle(\mathcal{R}-\langle\mathcal{R}\rangle)^3\rangle}{\langle(\mathcal{R}-\langle\mathcal{R}\rangle)^2\rangle^2} = \frac{6A^2B\sigma_{\delta\varphi}^4+8B^3\sigma_{\delta\varphi}^6}{A^4\sigma_{\delta\varphi}^4+4A^2B^2\sigma_{\delta\varphi}^6+4B^4\sigma_{\delta\varphi}^8} \simeq \begin{cases} \frac{18}{5}f_{\mathrm{NL}}^{\mathrm{local}} & (A \gg B\sigma_{\delta\varphi}) \\ \frac{2}{B\sigma_{\delta\varphi}^2} & (A \ll B\sigma_{\delta\varphi}) \end{cases} \tag{6.4}$$

For $A \ll B\sigma_{\delta\varphi}$ this ratio is not related to $f_{\mathrm{NL}}^{\mathrm{local}}$, while in the other limit they coincide up to an $\mathcal{O}(1)$ numerical factor. Figure 6 shows the variance, skewness and their ratio for γ around γ_0. Since γ corresponds to the scale k, they are closely connected to the power spectrum and the bispectrum of the curvature perturbation. Both of them has a dip at $\gamma=\gamma_0=0.3$ where the linear contribution from $\delta\varphi$ disappears (i.e. $A=0$). This corresponds to the dip in the power spectrum that frequently appears in PBH formation models [108]. In linear perturbation theory, $\delta\varphi^2$ is neglected, $\mathcal{R}$ would vanish from eq. (6.1), and the dip is infinitely deep at $\gamma=\gamma_0$.[8] In contrast, our result with the δN formalism indicates that the dip depth is finite due to the non-linear contribution. It has been reported that the inclusion of a loop correction results in a shallower dip [103], which is consistent with our result.

---

[7]This corresponds to the case where δN is always positive for any $|\delta\varphi|$ regardless of its sign. This means that the background trajectory passes through the step in the shortest time compared to all other perturbed trajectories.

[8]The dip would never become exactly zero in linear perturbation theory, which is in contradiction with our result. We suspect this is due to the neglection of the next leading order terms in gradient expansion in the δN formalism. In any case, since the nonlinear terms dominate the spectrum at the dip, this inaccuracy does not affect the conclusion that the deep dip disappears once nonlinear terms are included.
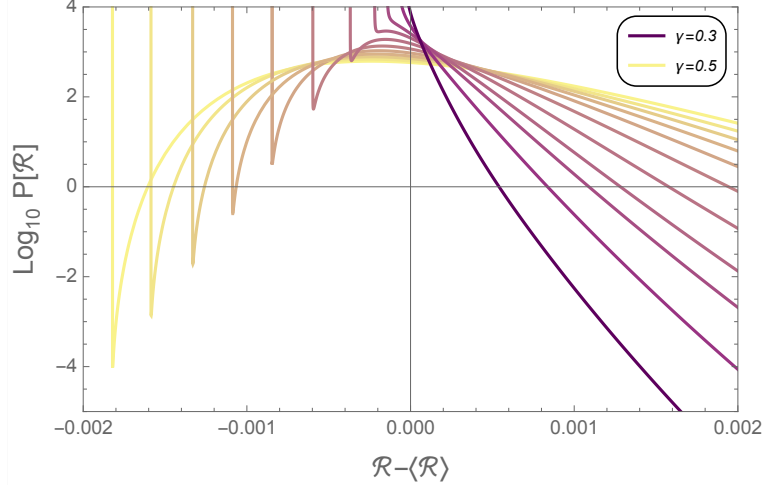
Figure 5. The PDFs of $\mathcal{R}$ against $\mathcal{R} - \langle \mathcal{R} \rangle$ for $\kappa = 1$, $\beta = 20$, $g = 0.02$, $\sigma_{\delta\varphi} = 5 \times 10^{-5}$ and $\omega_{s2} = 50$. γ, which corresponds to the scale of $\mathcal{R}$, varies from 0.5 (light yellow) to $\gamma_0 = 0.3$ (dark purple) with colour gradient. The probability density for negative $\mathcal{R}$ gradually disappears as the scale changes. The mean value is $\langle \mathcal{R} \rangle = \mathcal{O}(10^{-5})$. Each PDF is normalized so that the total probability is unity, and the contribution from the apparently diverging part at the lower end of the PDF is negligibly small.
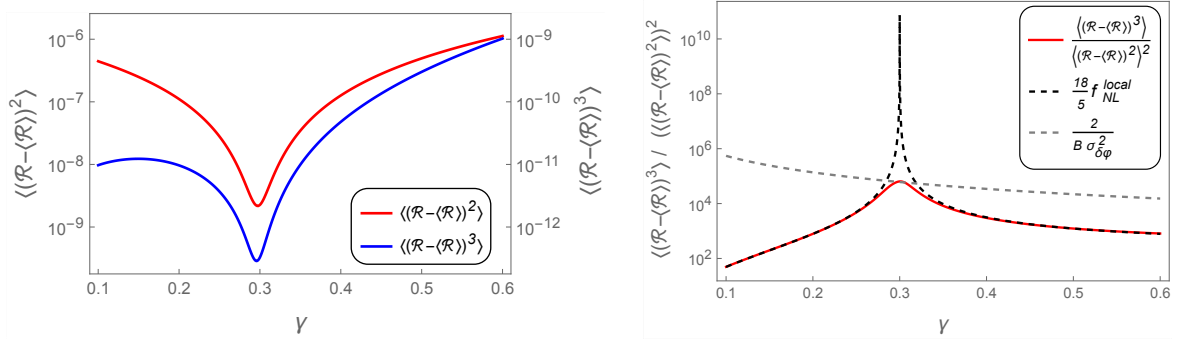

Figure 6. (Left panel) The variance $\langle (\mathcal{R} - \langle \mathcal{R} \rangle)^2 \rangle$ (red) and the skewness $\langle (\mathcal{R} - \langle \mathcal{R} \rangle)^3 \rangle$ (blue) of the curvature perturbation against γ representing the corresponding scale around $\gamma_0 = 0.3$. They have sharp dips at $\gamma = \gamma_0$ because the linear term in eq. (6.1) vanishes. (Right panel) The ratio of the these two $\langle (\mathcal{R} - \langle \mathcal{R} \rangle)^3 \rangle / \langle (\mathcal{R} - \langle \mathcal{R} \rangle)^2 \rangle$ compared to the asymptotic expressions, $2/B\sigma_{\delta\varphi}^2$ (gray dashed) and $18 f_{\mathrm{NL}}^{\mathrm{local}}/5$ (black dashed), given in eq. (6.4). They match at $\gamma = \gamma_0$ and at far region from it, respectively, as expected. The parameter choice is the same as figure 5.

In order to intuitively understand the consequence of the highly asymmetric PDF, we present figure 7 in which $\mathcal{R}$ is regarded as a classical stochastic quantity and its values are randomly assigned to lattices on a two-dimensional plane. $\mathcal{R}$ is probabilistically weighted by the Gaussian PDF in the left panel and the highly asymmetric PDF for $\gamma = \gamma_0$ in the right panel, respectively. It can be clearly seen that the distribution is biased to positive value in the highly asymmetric case compared to the Gaussian case. In the highly asymmetric case, $\mathcal{R}$ does not appear with large negative values because of $\mathcal{R}_{\min}$. When one interprets figure 7 as the spatial distribution of density fluctuations, this result would imply that there are fewer voids (low-density regions) than the normal Gaussian case. It would be interesting to consider such a signature in observation. We leave it for future study.
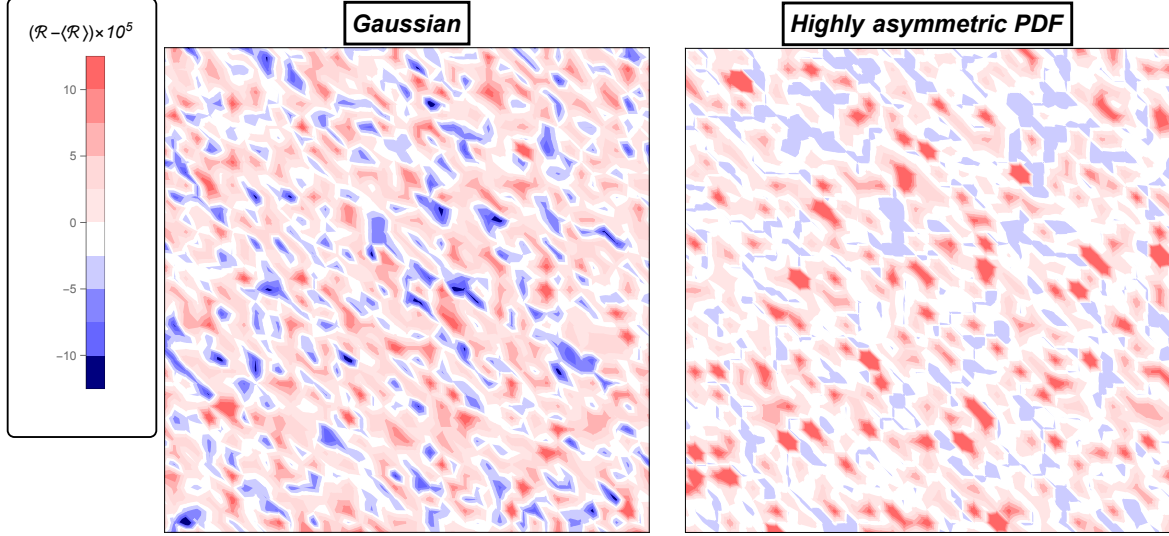
Figure 7. Illustration of the distributions of the curvature perturbation $\mathcal{R}$ based on different PDFs. $\mathcal{R}$ is randomly assigned to each of 40×40 two-dimensional lattice points according to the Gaussian PDF (left) and the asymmetric PDF with $\gamma = \gamma_0$ (right). Both panels use the same colour scheme, with red for high and blue for low value of $\mathcal{R}$. Identifying $\mathcal{R}$ with the density fluctuation, one can observe the spatial distribution of the primordial density contrast. In the Gaussian distribution, high and low density regions appear in equal proportions, whereas very low density regions (dark blue) are not found in the highly asymmetric PDF, which implies the distribution is significantly biased.

We expect that such asymmetric PDFs generically appear in models in which the inflaton experiences an accelerated SR phase, passes an inflection point, and subsequently enters a decelerated phase. This is because when we consider δN from the accelerated SR phase, it can become large and positive for both $\delta\varphi > 0$ and $\delta\varphi < 0$, which leads to the existence of $\mathcal{R}_{\min}$ in the same way as our model.

Assuming the inflaton φ is initially slow-rolling and moving toward the negative direction, the scalar field perturbation $\delta\varphi$ in the accelerated phase affects the velocity at the inflection point π_1 in such a way that its absolute value $|\pi_1 + \delta\pi_1|$ becomes larger for $\delta\varphi > 0$. Conversely, $|\pi_1 + \delta\pi_1|$ becomes smaller than $|\pi_1|$ for $\delta\varphi < 0$. For such trajectories it takes longer time to pass through the decelerated phase, which leads to large positive δN.

On the other hand, for $\delta\varphi > 0$, although the time to pass through the decelerated phase may become shorter by the increase in the absolute value of the velocity, depending on the values of the model parameters as well as on the scale of interest, the number of e-folds may eventually increase for sufficiently large $\delta\varphi$, as the perturbed trajectory starts at a greater distance from the inflection point. This gives rise to the appearance of $\mathcal{R}_{\min}$. In our model the condition that this happens is $\beta > \kappa\gamma/3$.

Furthermore, corresponding to the scale at which $\gamma = \gamma_0$ in our model, we expect that there is a scale at which δN is non-negative, regardless of the sign of $\delta\varphi$. This occurs when the term linear in $\delta\varphi$ vanishes. Apparently, the PDF in this case is highly asymmetric.

7 Conclusion

We studied an inflationary model in which the inflaton potential includes a finite-width upward step between two slow-roll stages. The inflaton loses its kinetic energy during the step stage where it climbs up the step, which has a large effect on the statistical distribution of the curvature perturbation. We derived the relation between the curvature perturbation $\mathcal{R}$ and the scalar field perturbation $\delta\varphi$ and obtained eq. (4.7) by using the δN formalism. We found that the step-width $\Delta\varphi$ plays a important role in the estimation of $\mathcal{R}$.

In section 5, we calculated the PDF of the curvature perturbation $\mathcal{R}$ and obtained eq. (5.1). The result is shown in figure 2. For $\mathcal{R} < \mathcal{R}_{\text{cutoff}} = \kappa g/3$ the PDF follows the Cutoff PDF given in eq. (5.2), while for $\mathcal{R} > \mathcal{R}_{\text{cutoff}} = \kappa g/3$ the exponential tail $P[\mathcal{R}] \propto \exp(-2\omega_{\text{s}2}\mathcal{R})$ is dominant. The slope of the tail depends on the step width $\Delta\varphi$ through $\omega_{\text{s}2} \simeq \sqrt{2}\,|\pi_1|/\Delta\varphi$. The CCDF was also calculated, and the significant impact on the PBH abundance of this exponential tail was illustrated in figure 3. We conclude that the step width should be taken into account for the accurate estimation of the PBH abundance.

In section 6 we discussed the highly asymmetric PDF. As shown in figure 4, for $\gamma > 0$ and $\beta > \kappa\gamma/3$, $\mathcal{R}$ has a minimum value $\mathcal{R}_{\text{min}}$. At a particular scale $\gamma = \gamma_0$ exiting the Hubble horizon before the step, $\mathcal{R}_{\text{min}}$ is realised with $\delta\varphi = 0$, which means that A as defined in eq. (6.2) vanishes and that $\mathcal{R}$ is supported by $\delta\varphi^2$ instead of $\delta\varphi$. We found that this scale γ_0 corresponds to the dip of the curvature power spectrum known in other models. On this scale, $f_{\text{NL}}^{\text{local}}$ formally diverges and the highly asymmetric PDF appears as shown in figures 5 and 6. The highly asymmetric PDF may result in a lower abundance of low-density regions such as voids (see figure 7) compared to the normal Gaussian case.

In this paper, we mainly investigated curvature perturbations on the scales exiting the Hubble horizon just before the background inflaton enters the step stage. It would also be interesting to calculate the PDF for scales exiting the Hubble horizon during and after the step stage for the comprehensive understanding of this model. In doing so, one needs to track the time evolution of $\delta\varphi$ more precisely, to include the contribution of $\delta\pi$, and to take into account the intrinsic non-gaussianity of $\delta\varphi$. As another approach, it is also fascinating to apply the stochastic-δN formalism to this upward step model. We leave these as future work.

A Parameters in f_{step}

The parameters in eq. (2.6) are determined by imposing the continuity conditions on the potential $v(\varphi)$ and its first derivative $\partial_\varphi v$ at $\varphi = \varphi_1, \varphi_2$ and φ_c. We then obtain the parameters of f_{step} as

$$A_1 = v_{\text{sr1}}(\varphi_1) - \frac{(\partial_\varphi v_{\text{sr1}}(\varphi_1))^2}{4B_1} , \tag{A.1}$$

$$A_2 = v_{\text{sr2}}(\varphi_2) - \frac{(\partial_\varphi v_{\text{sr2}}(\varphi_2))^2}{4B_2} , \tag{A.2}$$

$$B_1 = \frac{2\Delta v}{(\Delta\varphi)^2} + \frac{3\partial_\varphi v_{\text{sr1}}(\varphi_1) + \partial_\varphi v_{\text{sr2}}(\varphi_2)}{2\Delta\varphi} , \tag{A.3}$$

$$B_2 = -\frac{2\Delta v}{(\Delta\varphi)^2} - \frac{\partial_\varphi v_{\text{sr1}}(\varphi_1) + 3\partial_\varphi v_{\text{sr2}}(\varphi_2)}{2\Delta\varphi} , \tag{A.4}$$

$$\varphi_{\min} = \varphi_1 - \frac{\partial_\varphi v_{\text{sr1}}(\varphi_1)}{2B_1} , \tag{A.5}$$

$$\varphi_{\max} = \varphi_2 - \frac{\partial_\varphi v_{\text{sr2}}(\varphi_2)}{2B_2}, \tag{A.6}$$

where $\Delta v \equiv v_{\text{sr2}}(\varphi_2) - v_{\text{sr1}}(\varphi_1)$ corresponds to the height of the step.

B Solving background EOM

Here we solve the background equation of motion for the scalar field. In the following, we assume that the kinetic energy of the scalar field is subdominant compared to the potential energy, $h^2\pi^2 \ll v$, throughout the three stages (approximation (I) in section 3). This reduces the EOM (2.3) to

$$\frac{d\pi}{dn} + 3\pi + 3\frac{\partial_\varphi v}{v} = 0 . \tag{B.1}$$

We analytically solve this approximate EOM (B.1) in each of the three stages.

B.1 SR stages

In this subsection we discuss the dynamics before and after the step. The step stage will be addressed in the next subsections. In these stages, the potential is almost flat and the Taylor expansion is a sufficiently good approximation for the potential. To solve eq. (B.1) analytically, we expand the potential term up to the first order in the vicinity of $\varphi = \varphi_i$. Then, we obtain the equation of motion

$$\frac{d\pi}{dn} + 3\pi + 3\sqrt{2\epsilon_{Vi}} - \frac{3}{2}\eta_i(\varphi - \varphi_i) = 0 , \tag{B.2}$$

for $\varphi \geq \varphi_1$ ($i = 1$) and $\varphi \leq \varphi_2$ ($i = 2$), respectively. The solutions are

$$\varphi(n) - \varphi_i = C_i^+(\pi_i)e^{\lambda_i^+(n-n_i)} + C_i^-(\pi_i)e^{\lambda_i^-(n-n_i)} + \frac{2\sqrt{2\epsilon_{Vi}}}{\eta_i} , \tag{B.3}$$

where $\lambda_i^{\pm}$ and $C_i^{\pm}$ are constants for a given trajectory (i.e. for given boundary conditions at $n = n_i$),

$$\lambda_i^+ = -\frac{3}{2}\left(1 + \sqrt{1 + \frac{2\eta_i}{3}}\right) \simeq -3 - \frac{\eta_i}{2}, \tag{B.4}$$

$$\lambda_i^- = -\frac{3}{2}\left(1 - \sqrt{1 + \frac{2\eta_i}{3}}\right) \simeq \frac{\eta_i}{2}, \tag{B.5}$$

$$C_i^+(\pi_i) = \frac{1}{\lambda_i^+ - \lambda_i^-}\left(\pi_i + \lambda_i^- \frac{2\sqrt{2\epsilon_{Vi}}}{\eta_i}\right) \simeq -\frac{1}{3}\left(\pi_i + \sqrt{2\epsilon_{Vi}}\right), \tag{B.6}$$

$$C_i^-(\pi_i) = \frac{1}{\lambda_i^- - \lambda_i^+}\left(\pi_i + \lambda_i^+ \frac{2\sqrt{2\epsilon_{Vi}}}{\eta_i}\right) \simeq \frac{1}{3}\left(-\frac{6\sqrt{2\epsilon_{Vi}}}{\eta_i} + \pi_i + \sqrt{2\epsilon_{Vi}}\right). \tag{B.7}$$

For later discussion, we show π_2 with the first-order $\Delta\varphi$-corrections from the effect of the Hubble friction term. From the energy conservation law which includes the dissipation caused by the Hubble friction term, we obtain

$$\pi_2 = -\sqrt{\pi_1^2 - 6\log\left(\frac{v(\varphi_2)}{v(\varphi_1)}\right) - 6\int_{n_1}^{n_2}\pi^2(n)\mathrm{d}n} \tag{B.8}$$

$$\simeq -\sqrt{\pi_1^2 - 6\log\left(\frac{v(\varphi_2)}{v(\varphi_1)}\right) - 3\pi_1^2 N^{(\mathrm{s}1)} + 3\pi_c\Delta\varphi - 3\pi_2^2 N^{(\mathrm{s}2)}}, \tag{B.9}$$

where we used the zeroth-order solutions (3.3) and (3.4) to derive the second line. In eq. (B.8), the third term inside the square root corresponds to the dissipation term, which we ignored in the main context as the approximation (III) in section 3.

Note, however, that the last three terms in eq. (B.9) are not negligible compared to the sum of the first two terms for $\omega_{\mathrm{s}1}g^2 < 1$. Therefore, for the purpose of estimating π_2, the approximation (III) is not a good approximation. However, as we will see later in appendix D, the approximation (III) can be considered as a good approximation for estimating $\delta\pi_2$.

B.2 S1 region

Substituting eq. (2.6) into eq. (B.1) yields the equation of motion to be solved. To solve it analytically, we approximate the denominator of the third term in eq. (B.1) to be the constant value A_1 shown in eq. (A.1). This approximation is valid under the assumption that the step height Δv is sufficiently smaller than the value of the potential. Then the EOM is given by

$$\frac{\mathrm{d}\pi}{\mathrm{d}n} + 3\pi + \omega_{\mathrm{s}1}^2(\varphi - \varphi_{\min}) = 0. \tag{B.10}$$

Assuming $\omega_{\mathrm{s}1}^2 > 9/4$ and setting the values at $n = n_1$ as $\varphi = \varphi_1$ and $\pi = \pi_1$, the solution is

$$\varphi(n) - \varphi_{\min} = D_{\mathrm{s}1}e^{-\frac{3}{2}(n-n_1)}\sin\left(\sqrt{\omega_{\mathrm{s}1}^2 - \frac{9}{4}}(n - n_1) + \theta_{\mathrm{s}1}\right), \tag{B.11}$$

where D_{s1} and θ_{s1} are constants for a given trajectory, defined by

$$D_{s1} = -\sqrt{\frac{\pi_1^2 + 3\pi_1(\varphi_1 - \varphi_{\min}) + \omega_{s1}^2(\varphi_1 - \varphi_{\min})^2}{\omega_{s1}^2 - \frac{9}{4}}}, \tag{B.12}$$

$$\cos\theta_{s1} = \frac{\pi_1 + \frac{3}{2}(\varphi_1 - \varphi_{\min})}{D_{s1}\sqrt{\omega_{s1}^2 - \frac{9}{4}}} \quad \text{and} \quad \sin\theta_{s1} = \frac{\varphi_1 - \varphi_{\min}}{D_{s1}}. \tag{B.13}$$

Here we check that if $\Delta\varphi$ is sufficiently small, eq. (B.11) coincides with the solution, eq. (3.3), obtained from the approximated EOM to which approximations (II) and (III) are applied. For this purpose, it is sufficient to compare $\omega_{s1}^2(\varphi_1 - \varphi_{\min})^2$ to π_1^2,

$$\frac{\omega_{s1}^2(\varphi_1 - \varphi_{\min})^2}{\pi_1^2} = \frac{3(\partial_\varphi v_{sr1}(\varphi_1))^2}{2A_1B_1\pi_1^2} \simeq \frac{3}{4}\frac{(\partial_\varphi v_{sr1}(\varphi_1))^2}{v_{sr1}(\varphi_1)}\frac{(\Delta\varphi)^2}{\pi_1^2\Delta v} \sim 9\epsilon_{V1}\frac{(\Delta\varphi)^2}{\pi_1^4} = \mathcal{O}\!\left(\frac{1}{\omega_{s1}^2}\right), \tag{B.14}$$

where we used the approximation $\Delta v \sim v_{sr1}(\varphi_1)\pi_1^2/6$, which can be derived by the energy conservation law (3.2). From eq. (B.14), it follows that if ω_{s1} is much larger than 1, D_{s1}, θ_{s1} and $\varphi_{\min}$ are reduced to π_1/ω_{s1}, 0 and φ_1, respectively, i.e. eq. (3.3) is reproduced from eq. (B.11).

B.3   S2 region

Similarly, for the S2 region, the EOM to be solved is

$$\frac{d\pi}{dn} + 3\pi - \omega_{s2}^2(\varphi - \varphi_{\max}) = 0, \tag{B.15}$$

where we used the fact that B_2 is a negative value. Setting the values at $n = n_2$ as $\varphi = \varphi_2$ and $\pi = \pi_2$, the solution is

$$\varphi(n) - \varphi_{\max} = D_{s2}e^{-\frac{3}{2}(n-n_2)}\sinh\!\left(\sqrt{\omega_{s2}^2 + \frac{9}{4}}(n - n_2) + \theta_{s2}\right), \tag{B.16}$$

where D_{s2} and θ_{s2} are constants for a given trajectory, defined by

$$D_{s2} = -\sqrt{\frac{\pi_2^2 + 3\pi_2(\varphi_2 - \varphi_{\max}) - \omega_{s2}^2(\varphi_2 - \varphi_{\max})^2}{\omega_{s2}^2 + \frac{9}{4}}}, \tag{B.17}$$

$$\theta_{s2} = \log\!\left[\frac{1}{D_{s2}\sqrt{\omega_{s2}^2 + \frac{9}{4}}}\left(\pi_2 + \left(\frac{3}{2} + \sqrt{\omega_{s2}^2 + \frac{9}{4}}\right)(\varphi_2 - \varphi_{\max})\right)\right]. \tag{B.18}$$

Similar to eq. (B.14), we compare $\omega_{s2}^2(\varphi_2 - \varphi_{\max})^2$ to π_2^2 to find a condition under which eq. (3.4) is reproduced. We obtain

$$\frac{\omega_{s2}^2(\varphi_2 - \varphi_{\max})^2}{\pi_2^2} \simeq \frac{3}{4}\frac{(\partial_\varphi v_{sr2}(\varphi_2))^2}{v_{sr2}(\varphi_2)}\frac{(\Delta\varphi)^2}{\pi_2^2\Delta v} \sim 9\epsilon_{V2}\frac{(\Delta\varphi)^2}{\pi_1^2\pi_2^2} = \mathcal{O}\!\left(\frac{1}{\kappa^2 g^2\omega_{s2}^2}\right), \tag{B.19}$$

where we used the approximation $\Delta v \sim v_{sr2}(\varphi_2)\pi_1^2/6$. Thus, if $\kappa g\omega_{s2} \gg 1$ is satisfied, then D_{s2}, θ_{s2} and $\varphi_{\max}$ can be approximated by π_2/ω_{s2}, 0 and φ_2 and eq. (B.16) reduces to eq. (3.4).

C Derivation of δN in each stage

C.1 First SR stage

In the first SR stage the background trajectory is on the SR attractor. From eq. (B.3), we have

$$\varphi - \varphi_1 = -\frac{2\sqrt{2\epsilon_{V1}}}{\eta_1}e^{-\lambda_1^- N^{(1)}} + \frac{2\sqrt{2\epsilon_{V1}}}{\eta_1}, \tag{C.1}$$

$$\pi = -\sqrt{2\epsilon_{V1}} + \frac{\eta_1}{2}(\varphi - \varphi_1), \tag{C.2}$$

where $N^{(1)} \equiv N(\varphi, \pi; \varphi_1, \pi_1)$.

Now, what we are here to discuss is the deviation from the SR attractor, thus it is not sufficient just to perturb the background solutions (C.1) and (C.2). Replacing π_1 with $\pi_1 + \delta\pi_1$ in $C_1^\pm$, eq. (B.3) gives a perturbed trajectory,

$$\varphi(n) - \varphi_1 = C_1^+(\pi_1 + \delta\pi_1)e^{\lambda_1^+(n-n_1')} + C_1^-(\pi_1 + \delta\pi_1)e^{\lambda_1^-(n-n_1')} + \frac{2\sqrt{2\epsilon_{V1}}}{\eta_1}, \tag{C.3}$$

$$\pi(n) = C_1^+(\pi_1 + \delta\pi_1)\lambda_1^+ e^{\lambda_1^+(n-n_1')} + C_1^-(\pi_1 + \delta\pi_1)\lambda_1^- e^{\lambda_1^-(n-n_1')}, \tag{C.4}$$

which correspond to a trajectory passing through $(\varphi_1, \pi_1 + \delta\pi_1)$ at $n = n_1'$. We assign $\delta\varphi$ so that, in the phase space, $(\varphi + \delta\varphi, \pi)$ lies on the perturbed trajectory given by eqs. (C.3) and (C.4). Note that $\delta\varphi$ is uniquely determined by $\delta\pi_1$. Conversely, $\delta\pi_1$ should not be chosen such that there is no corresponding $\delta\varphi$. This allows us to substitute $\varphi(n') = \varphi + \delta\varphi$ and $\pi(n') = \pi$ into eqs. (C.3) and (C.4) as values at $n = n'$. Then, solving the system of equations for $e^{\lambda_1^+(n'-n_1')}$ and $e^{\lambda_1^-(n'-n_1')}$, we obtain

$$\delta\pi_1 \simeq -\lambda_1^- \delta\varphi e^{\lambda_1^+ \mathcal{N}^{(1)}}, \tag{C.5}$$

$$\delta\pi_1 \simeq \left(-\lambda_1^+ \delta\varphi + \left(1 - \frac{\lambda_1^+}{\lambda_1^-}\right)\pi_*\right)e^{\lambda_1^- \mathcal{N}^{(1)}} - \left(1 - \frac{\lambda_1^+}{\lambda_1^-}\right)\pi_1, \tag{C.6}$$

where $\mathcal{N}^{(1)} \equiv N(\varphi + \delta\varphi, \pi; \varphi_1, \pi_1 + \delta\pi_1) = n_1' - n'$. To derive these results, we used the background solution (C.2) and $\pi_1 = -\sqrt{2\epsilon_{V1}}$.

What we need to know in particular is the relation to $\delta\varphi$ for each of $\delta\pi_1$ and $\delta N^{(1)}(\equiv \mathcal{N}^{(1)} - N^{(1)})$. In principle, it is possible to solve them because there are two equations for two unknown quantities. However, since this system of equations contains two exponential functions, it is not possible to obtain an explicit form of the analytic solution. In order to solve them analytically, we limit our discussion to considering only the case in which $\delta N^{(1)}$ is sufficiently small, and perform an approximation that ignores second and higher orders for $\delta N^{(1)}$ and $\delta\varphi$. That is, the exponential functions in eqs. (C.5) and (C.6) are approximately

$$e^{\lambda_1^\pm \mathcal{N}^{(1)}} = e^{\lambda_1^\pm N^{(1)}}e^{\lambda_1^\pm \delta N^{(1)}} \simeq \left(\frac{\pi_1}{\pi}\right)^{\frac{\lambda_1^\pm}{\lambda_1^-}}\left(1 + \lambda_1^\pm \delta N^{(1)}\right), \tag{C.7}$$

where we used $e^{\lambda_1^- N^{(1)}} \simeq \pi_1/\pi$, which is derived from eqs. (C.1) and (C.2). Notice that this approximation (C.7) is only valid if $|\delta N^{(1)}| \ll 1/3$ is satisfied. This then makes it possible to

solve the system of equations analytically, and the final results can be obtained as

$$\delta\pi_1 \simeq -\lambda_1^- \left(\frac{\pi_1}{\pi}\right)^{\frac{\lambda_1^+}{\lambda_1^-}} \delta\varphi \simeq -\frac{\eta_1}{2}\left(\frac{\pi}{\pi_1}\right)^{\frac{6}{\eta_1}} \delta\varphi \,, \tag{C.8}$$

$$\delta N^{(1)} \simeq \frac{\lambda_1^+ - \lambda_1^-\left(\frac{\pi}{\pi_1}\right)^{1-\frac{\lambda_1^+}{\lambda_1^-}}}{\lambda_1^- - \lambda_1^+} \frac{\delta\varphi}{\pi} \simeq -\frac{\delta\varphi}{\pi} \,. \tag{C.9}$$

Note that in the above discussion $\delta N^{(1)}$ is limited to being small, but $N^{(1)}$ is not limited at all.

C.2 Second SR stage

By solving eq. (B.3) for $\varphi \leq \varphi_2$ in conjunction with the equation for π derived by differentiating eq. (B.3) with respect to n, we obtain $N^{(2)}(\equiv N(\varphi_2, \pi_2; \varphi_f, \pi_f) = n_f - n_2)$ as

$$N^{(2)} \simeq \frac{1}{\lambda_2^-} \log\left(\frac{\left(1 - \frac{\lambda_2^+}{\lambda_2^-}\right)\pi_f}{\pi_2 + \frac{\lambda_2^+}{\lambda_2^-}\sqrt{2\epsilon_{V2}}}\right) \,, \tag{C.10}$$

where π_f is the value of π at $n = n_f$. Replacing π_2 with $\pi_2 + \delta\pi_2$ in $C_2^\pm$, eq. (B.3) gives a perturbed trajectory. We can immediately obtain

$$\mathcal{N}^{(2)} \simeq \frac{1}{\lambda_2^-} \log\left(\frac{\left(1 - \frac{\lambda_2^+}{\lambda_2^-}\right)(\pi_f + \delta\pi_f)}{\pi_2 + \delta\pi_2 + \frac{\lambda_2^+}{\lambda_2^-}\sqrt{2\epsilon_{V2}}}\right) \,, \tag{C.11}$$

where $\mathcal{N}^{(2)} \equiv N(\varphi_2, \pi_2 + \delta\pi_2; \varphi_f, \pi_f)$. Recall that we ignore $\delta\pi_f$ by choosing n_f as the time later than which the trajectory converges to the SR attractor. Then $\delta N^{(2)}$ is given by

$$\delta N^{(2)} \equiv \mathcal{N}^{(2)} - N^{(2)} \simeq -\frac{1}{\lambda_2^-} \log\left(1 + \frac{\frac{\delta\pi_2}{\pi_2}}{1 - \frac{\lambda_2^+}{\lambda_2^-}\frac{1}{\kappa g}}\right) \simeq -\frac{\kappa g}{3}\frac{\delta\pi_2}{\pi_2} \,. \tag{C.12}$$

Note that the last approximate equality in eq. (C.12) is an approximation due to the fact that $|\lambda_2^+/\lambda_2^-|$ is much larger than 1, not that $\delta\pi_2/\pi_2$ is small. Substituting eq. (4.3) into eq. (C.12) leads to eq. (4.4), but note that eq. (4.3) ignores the Hubble friction. In appendix D, we will discuss the validity of eq. (4.3).

C.3 Step stage

First, let us estimate the number of e-folds in the S1 region. Assuming that $\Delta\varphi$ is sufficiently small, i.e. $\omega_{s1} \gg 1$, eq. (B.11) gives

$$-\frac{1}{2}\Delta\varphi \simeq \frac{\pi_1}{\omega_{s1}} e^{-\frac{3}{2}N^{(s1)}} \sin\left(\omega_{s1} N^{(s1)}\right) \,, \tag{C.13}$$

where $N^{(s1)} \equiv N(\varphi_1, \pi_1; \varphi_c, \pi_c) = n_c - n_1$. The scalar field should not oscillate around the local minimum of the potential as it climbs through the step. This fact tells us that

$$N^{(s1)} \leq \frac{\pi}{2\omega_{s1}} \ll 1 \,, \tag{C.14}$$

where we used that ω_{s1} is an inverse power of the order of $\Delta\varphi$ and is very large compared to 1. In this context, since the damping factor $\exp(-3N^{(s1)}/2)$ is approximately equal to 1, we have

$$N^{(s1)} \simeq \frac{1}{\omega_{s1}} \arcsin\left(-\frac{\Delta\varphi}{2\pi_1}\omega_{s1}\right). \tag{C.15}$$

Then varying $N^{(s1)}$ with respect to $\delta\pi_1$ yields

$$\delta N^{(s1)} = -\frac{1}{2}\frac{\Delta\varphi}{\sqrt{\pi_1^2 - \left(\frac{1}{2}\Delta\varphi\omega_{s1}\right)^2}}\frac{\delta\pi_1}{\pi_1} \simeq -\frac{1}{\omega_{s1}}\frac{\delta\pi_1}{\pi_1} \simeq -\frac{\eta_1}{2\omega_{s1}}\left(\frac{\pi}{\pi_1}\right)^{1+\frac{6}{\eta_1}}\delta N^{(1)}. \tag{C.16}$$

Here, $\delta\pi_1/\pi_1$ is assumed to be much smaller than 1, and $\delta N^{(s1)}$ is expanded up to the first order of $\delta\pi_1/\pi_1$. It can be seen that $\delta N^{(s1)}$ is strongly suppressed by $\Delta\varphi$ and $(\pi/\pi_1)^{1+\frac{6}{\eta_1}}$ compared to $\delta N^{(1)}$. For this reason, we have ignored $\delta N^{(s1)}$ in the main part of the paper.

The number of e-folds for the S2 region can then be calculated by imposing the same condition, i.e., $\Delta\varphi$ is small (quantitatively, $\Delta\varphi \ll \kappa g|\pi_1|$). Since ω_{s2} is considerably larger than $3/2$, the damping factor $e^{-3(n-n_2)/2}$ in eq. (B.16) is negligible. Under this approximation, eq. (B.16) can be solved inversely for $N^{(s2)} \equiv N(\varphi_c, \pi_c; \varphi_2, \pi_2) = n_2 - n_c$, and it yields

$$N^{(s2)} \simeq \frac{1}{\omega_{s2}}\sinh^{-1}\left(\frac{\Delta\varphi}{2|\pi_2|}\omega_{s2}\right) \simeq \frac{1}{\omega_{s2}}\log\left(\frac{\Delta\varphi}{|\pi_2|}\omega_{s2}\right). \tag{C.17}$$

The number of e-folds in the perturbed trajectory, $\mathcal{N}^{(s2)} \equiv N(\varphi_c, \pi_c + \delta\pi_c; \varphi_2, \pi_2 + \delta\pi_2)$, is also represented in the same form. As a result, we obtain

$$\delta N^{(s2)} \simeq -\frac{1}{\omega_{s2}}\log\left(1 + \frac{\delta\pi_2}{\pi_2}\right). \tag{C.18}$$

It is important to note that this may not be just a correction term. Certainly $1/\omega_{s2}$ is of the order of $\Delta\varphi$, however when $\delta\pi_2$ is comparable to $-\pi_2$, $\delta N^{(s2)}$ may diverge to infinity. This is a consequence of the existence of perturbed trajectories that barely reach the local maximum of the potential and take an enormous amount of time to pass through the step. Therefore, the contribution to the total δN from $\delta N^{(s2)}$ cannot be ignored and must be taken into account.

D   Hubble friction corrections during step stage

In the main text we imposed the approximation condition (Ⅲ) and neglected the Hubble friction during the step stage. However, as we have seen in appendix B.1, the $\mathcal{O}(\Delta\varphi)$ corrections are not necessarily negligible compared to the zeroth orders in the background solution, since the first and second terms in eq. (B.9) largely cancel each other out for small g. In this section we verify that they are negligible at the perturbation level and that eq. (4.3) is a good enough approximation.

From eq. (B.9), we can obtain

$$\pi_2 + \delta\pi_2 = \pi_2\left[1 + \frac{2}{g^2}\frac{\delta\pi_1}{\pi_1} + \frac{1}{g^2}\left(\frac{\delta\pi_1}{\pi_1}\right)^2 - \frac{3}{g^2}\left(1 + \frac{\delta\pi_1}{\pi_1}\right)^2\delta N^{(s1)} - \frac{3\delta\pi_1}{g^2\pi_1}\left(2 + \frac{\delta\pi_1}{\pi_1}\right)N^{(s1)}\right.$$

$$\left. + \frac{3\Delta\varphi}{g^2}\delta\pi_c - 3\left(1 + \frac{\delta\pi_2}{\pi_2}\right)^2(N^{(s2)} + \delta N^{(s2)}) + 3N^{(s2)}\right]^{\frac{1}{2}}. \tag{D.1}$$

In the following, for simplicity, the second and higher orders of $\delta\pi_1/\pi_1$ are truncated. This is well justified for $g \ll 1$. Substituting the already calculated $\Delta\varphi$ zeroth order solutions (C.15), (C.16), (C.17), (C.18) and (4.3) into eq. (D.1), we obtain

$$\pi_2 + \delta\pi_2 = \pi_2 \left[1 + \frac{2}{g^2} \frac{\delta\pi_1}{\pi_1} - \frac{3}{g^2} \delta N^{(\mathrm{s}1)} - \frac{6\delta\pi_1}{g^2\pi_1} N^{(\mathrm{s}1)} + \frac{3\Delta\varphi}{g^2\pi_c} \frac{\delta\pi_1}{\pi_1} - \frac{6\delta\pi_1}{g^2\pi_1} N^{(\mathrm{s}2)} - 3\left(1 + \frac{\delta\pi_2}{\pi_2}\right)^2 \delta N^{(\mathrm{s}2)} \right]^{\frac{1}{2}}$$

$$\simeq \pi_2 \left[1 + \frac{2}{g^2}\left(1 - \frac{3}{2\omega_{\mathrm{s}1}} + \frac{3\Delta\varphi}{2\pi_c} - \frac{3}{\omega_{\mathrm{s}2}}\log\left(\frac{\sqrt{2}}{g}\right)\right)\frac{\delta\pi_1}{\pi_1} + \frac{3}{2\omega_{\mathrm{s}2}}\left(1 + \frac{2}{g^2}\frac{\delta\pi_1}{\pi_1}\right)\log\left(1 + \frac{2}{g^2}\frac{\delta\pi_1}{\pi_1}\right) \right]^{\frac{1}{2}}.$$
$$(\mathrm{D.2})$$

Therefore, if the step width is sufficiently small, i.e. $\omega_{\mathrm{s}1}, \omega_{\mathrm{s}2} \gg 1$ and $\omega_{\mathrm{s}2} \gg |3\log g|$, the $\Delta\varphi$ corrections are subdominant and negligible. In this case, the Hubble friction can be ignored when calculating $\delta\pi_2$ with g as an input parameter, resulting in eq. (4.3) being a good approximation.

E Derivation of PDF for each case

Using eq. (5.1), we can numerically obtain the PDF of $\mathcal{R}$. However, since it is not possible to solve eq. (4.7) analytically, we cannot obtain the analytically explicit form of the PDF in terms of $\mathcal{R}$. Instead of solving eq. (4.7) exactly, it may be useful to derive the shape of the PDF in each case where one term in eq. (4.7) makes a larger contribution than others, in order to understand the specific features of the full PDF in this model. For simplicity, in the following discussion we assume that $g \ll 1$, otherwise the PDF in our model becomes close to the Gaussian case.

1. *The linear perturbative regime.* In this case, the PDF is obviously given by a Gaussian distribution with variance $\sigma_{\mathcal{R}}^2 = (\beta - \kappa\gamma/3g - \gamma/\omega_{\mathrm{s}2}g^2)^2 \sigma_{\delta\varphi}^2$, namely,

$$P[\mathcal{R}] = \frac{1}{\sqrt{2\pi\left(\beta - \frac{\kappa\gamma}{3g} - \frac{\gamma}{\omega_{\mathrm{s}2}g^2}\right)^2 \sigma_{\delta\varphi}^2}} \exp\left(-\frac{\mathcal{R}^2}{2\left(\beta - \frac{\kappa\gamma}{3g} - \frac{\gamma}{\omega_{\mathrm{s}2}g^2}\right)^2 \sigma_{\delta\varphi}^2}\right). \qquad (\mathrm{E.1})$$

2. *The second term dominant regime.* Based on the assumption $g \ll 1$, we can ignore the third term in the square root in the second term of eq. (4.7), i.e.

$$\mathcal{R} \simeq \frac{\kappa g}{3}\left(1 - \sqrt{1 + \frac{2\gamma}{g^2}\delta\varphi}\right). \qquad (\mathrm{E.2})$$

The inverse of this equation gives us

$$\delta\varphi \simeq \frac{9}{2}\frac{\mathcal{R}^2}{\gamma\kappa^2} - 3\frac{g\mathcal{R}}{\gamma\kappa}, \qquad (\mathrm{E.3})$$

and the PDF is

$$P[\mathcal{R}] = \frac{1}{\sqrt{2\pi\sigma_{\delta\varphi}^2}}\frac{3g}{|\gamma|\kappa}\left(1 - \frac{3\mathcal{R}}{g\kappa}\right)\exp\left[-\frac{1}{2\sigma_{\delta\varphi}^2}\frac{9g^2\mathcal{R}^2}{\gamma^2\kappa^2}\left(1 - \frac{3}{2}\frac{\mathcal{R}}{g\kappa}\right)^2\right]. \qquad (\mathrm{E.4})$$

We note that in this case there is a cutoff at $\mathcal{R} = \kappa g/3$. It can be seen that the PDF decreases rapidly towards 0 at $\mathcal{R} = \kappa g/3$ due to the factor $1 - 3\mathcal{R}/g\kappa$. Since the cutoff depends not only on κ but also on g, the smaller g we choose, the smaller the cutoff tends to be.

3. *The third term dominant regime.* Around $\delta\varphi \simeq -2\gamma/g^2$, the main contribution to $\mathcal{R}$ is the third term in eq. (4.7), namely,

$$\mathcal{R} \simeq -\frac{1}{2\omega_{\mathrm{s}2}} \log\left(1 + \frac{2\gamma}{g^2}\delta\varphi\right). \tag{E.5}$$

Thus $\delta\varphi$ can be given by

$$\delta\varphi \simeq \frac{g^2}{2\gamma}\Big(\exp(-2\omega_{\mathrm{s}2}\mathcal{R}) - 1\Big), \tag{E.6}$$

and then the PDF is

$$P[\mathcal{R}] = \frac{1}{\sqrt{2\pi\sigma_{\delta\varphi}^2}}\frac{g^2\omega_{\mathrm{s}2}}{|\gamma|}\exp(-2\omega_{\mathrm{s}2}\mathcal{R})\exp\left[-\frac{1}{2\sigma_{\delta\varphi}^2}\frac{g^2}{4\gamma^2}\Big(\exp(-2\omega_{\mathrm{s}2}\mathcal{R}) - 1\Big)^2\right]. \tag{E.7}$$

For a sufficiently large $\mathcal{R}$, this PDF is almost proportional to $\exp(-2\omega_{\mathrm{s}2}\mathcal{R})$, i.e. the tail appears. Recalling that $\omega_{\mathrm{s}2} \propto 1/\Delta\varphi$, we can see that the effect of this tail is suppressed by $\Delta\varphi$. If we take the case of zero width limit, $\Delta\varphi = 0$, then the tail vanishes and the cutoff described in refs. [81, 82] can be reproduced. However, the PDF is nonzero even for $\mathcal{R}$ larger than the cutoff value, $\mathcal{R}_{\mathrm{cutoff}} = \kappa g/3$, unless $\Delta\varphi$ is exactly zero. In this sense, we can conclude that the cutoff is a side effect of ignoring the finite step width.

References

[1] A.A. Starobinsky, *A New Type of Isotropic Cosmological Models Without Singularity*, *Phys. Lett. B* **91** (1980) 99 [InSPIRE].

[2] K. Sato, *First Order Phase Transition of a Vacuum and Expansion of the Universe*, *Mon. Not. Roy. Astron. Soc.* **195** (1981) 467 [InSPIRE].

[3] D. Kazanas, *Dynamics of the Universe and Spontaneous Symmetry Breaking*, *Astrophys. J. Lett.* **241** (1980) L59 [InSPIRE].

[4] A.H. Guth, *The Inflationary Universe: A Possible Solution to the Horizon and Flatness Problems*, *Phys. Rev. D* **23** (1981) 347 [InSPIRE].

[5] A.D. Linde, *A New Inflationary Universe Scenario: A Possible Solution of the Horizon, Flatness, Homogeneity, Isotropy and Primordial Monopole Problems*, *Phys. Lett. B* **108** (1982) 389 [InSPIRE].

[6] A. Albrecht and P.J. Steinhardt, *Cosmology for Grand Unified Theories with Radiatively Induced Symmetry Breaking*, *Phys. Rev. Lett.* **48** (1982) 1220 [InSPIRE].

[7] PLANCK collaboration, *Planck 2018 results. VI. Cosmological parameters*, *Astron. Astrophys.* **641** (2020) A6 [*Erratum ibid.* **652** (2021) C4] [`arXiv:1807.06209`] [InSPIRE].

[8] PLANCK collaboration, *Planck 2018 results. X. Constraints on inflation*, *Astron. Astrophys.* **641** (2020) A10 [`arXiv:1807.06211`] [InSPIRE].

[9] A.D. Linde, *Chaotic Inflation*, *Phys. Lett. B* **129** (1983) 177 [ɪɴSPIRE].

[10] K. Freese, J.A. Frieman and A.V. Olinto, *Natural inflation with pseudo — Nambu-Goldstone bosons*, *Phys. Rev. Lett.* **65** (1990) 3233 [ɪɴSPIRE].

[11] F.L. Bezrukov and M. Shaposhnikov, *The Standard Model Higgs boson as the inflaton*, *Phys. Lett. B* **659** (2008) 703 [arXiv:0710.3755] [ɪɴSPIRE].

[12] R. Kallosh, A. Linde and D. Roest, *Superconformal Inflationary α-Attractors*, *JHEP* **11** (2013) 198 [arXiv:1311.0472] [ɪɴSPIRE].

[13] Y.B. Zel'dovich and I.D. Novikov, *The Hypothesis of Cores Retarded during Expansion and the Hot Cosmological Model*, *Sov. Astron.* **10** (1967) 602 [ɪɴSPIRE].

[14] S. Hawking, *Gravitationally collapsed objects of very low mass*, *Mon. Not. Roy. Astron. Soc.* **152** (1971) 75 [ɪɴSPIRE].

[15] B.J. Carr and S.W. Hawking, *Black holes in the early Universe*, *Mon. Not. Roy. Astron. Soc.* **168** (1974) 399 [ɪɴSPIRE].

[16] B.J. Carr, *The Primordial black hole mass spectrum*, *Astrophys. J.* **201** (1975) 1 [ɪɴSPIRE].

[17] J. García-Bellido and E. Ruiz Morales, *Primordial black holes from single field models of inflation*, *Phys. Dark Univ.* **18** (2017) 47 [arXiv:1702.03901] [ɪɴSPIRE].

[18] K. Kannike, L. Marzola, M. Raidal and H. Veermäe, *Single Field Double Inflation and Primordial Black Holes*, *JCAP* **09** (2017) 020 [arXiv:1705.06225] [ɪɴSPIRE].

[19] C. Germani and T. Prokopec, *On primordial black holes from an inflection point*, *Phys. Dark Univ.* **18** (2017) 6 [arXiv:1706.04226] [ɪɴSPIRE].

[20] J.M. Ezquiaga, J. García-Bellido and E. Ruiz Morales, *Primordial Black Hole production in Critical Higgs Inflation*, *Phys. Lett. B* **776** (2018) 345 [arXiv:1705.04861] [ɪɴSPIRE].

[21] H. Motohashi and W. Hu, *Primordial Black Holes and Slow-Roll Violation*, *Phys. Rev. D* **96** (2017) 063503 [arXiv:1706.06784] [ɪɴSPIRE].

[22] M.Y. Khlopov, *Primordial Black Holes*, *Res. Astron. Astrophys.* **10** (2010) 495 [arXiv:0801.0116] [ɪɴSPIRE].

[23] M. Sasaki, T. Suyama, T. Tanaka and S. Yokoyama, *Primordial black holes — perspectives in gravitational wave astronomy*, *Class. Quant. Grav.* **35** (2018) 063001 [arXiv:1801.05235] [ɪɴSPIRE].

[24] B. Carr and F. Kuhnel, *Primordial Black Holes as Dark Matter: Recent Developments*, *Ann. Rev. Nucl. Part. Sci.* **70** (2020) 355 [arXiv:2006.02838] [ɪɴSPIRE].

[25] A.M. Green and B.J. Kavanagh, *Primordial Black Holes as a dark matter candidate*, *J. Phys. G* **48** (2021) 043001 [arXiv:2007.10722] [ɪɴSPIRE].

[26] B. Carr, K. Kohri, Y. Sendouda and J. Yokoyama, *Constraints on primordial black holes*, *Rept. Prog. Phys.* **84** (2021) 116902 [arXiv:2002.12778] [ɪɴSPIRE].

[27] P. Villanueva-Domingo, O. Mena and S. Palomares-Ruiz, *A brief review on primordial black holes as dark matter*, *Front. Astron. Space Sci.* **8** (2021) 87 [arXiv:2103.12087] [ɪɴSPIRE].

[28] B. Carr and F. Kuhnel, *Primordial black holes as dark matter candidates*, *SciPost Phys. Lect. Notes* **48** (2022) 1 [arXiv:2110.02821] [ɪɴSPIRE].

[29] A. Escrivà, F. Kuhnel and Y. Tada, *Primordial Black Holes*, arXiv:2211.05767 [ɪɴSPIRE].

[30] A. Karam et al., *Anatomy of single-field inflationary models for primordial black holes*, *JCAP* **03** (2023) 013 [`arXiv:2205.13540`] [ɪɴSPIRE].

[31] O. Özsoy and G. Tasinato, *Inflation and Primordial Black Holes*, *Universe* **9** (2023) 203 [`arXiv:2301.03600`] [ɪɴSPIRE].

[32] E. Komatsu and D.N. Spergel, *Acoustic signatures in the primary microwave background bispectrum*, *Phys. Rev. D* **63** (2001) 063002 [`astro-ph/0005036`] [ɪɴSPIRE].

[33] N. Bartolo, S. Matarrese and A. Riotto, *Nongaussianity from inflation*, *Phys. Rev. D* **65** (2002) 103505 [`hep-ph/0112261`] [ɪɴSPIRE].

[34] J.M. Maldacena, *Non-Gaussian features of primordial fluctuations in single field inflationary models*, *JHEP* **05** (2003) 013 [`astro-ph/0210603`] [ɪɴSPIRE].

[35] V. Acquaviva, N. Bartolo, S. Matarrese and A. Riotto, *Second order cosmological perturbations from inflation*, *Nucl. Phys. B* **667** (2003) 119 [`astro-ph/0209156`] [ɪɴSPIRE].

[36] N. Bartolo, E. Komatsu, S. Matarrese and A. Riotto, *Non-Gaussianity from inflation: Theory and observations*, *Phys. Rept.* **402** (2004) 103 [`astro-ph/0406398`] [ɪɴSPIRE].

[37] X. Chen, *Primordial Non-Gaussianities from Inflation Models*, *Adv. Astron.* **2010** (2010) 638979 [`arXiv:1002.1416`] [ɪɴSPIRE].

[38] M.H. Namjoo, H. Firouzjahi and M. Sasaki, *Violation of non-Gaussianity consistency relation in a single field inflationary model*, *EPL* **101** (2013) 39001 [`arXiv:1210.3692`] [ɪɴSPIRE].

[39] X. Chen, H. Firouzjahi, M.H. Namjoo and M. Sasaki, *A Single Field Inflation Model with Large Local Non-Gaussianity*, *EPL* **102** (2013) 59001 [`arXiv:1301.5699`] [ɪɴSPIRE].

[40] X. Chen et al., *In-in and δN calculations of the bispectrum from non-attractor single-field inflation*, *JCAP* **12** (2013) 039 [`arXiv:1308.5341`] [ɪɴSPIRE].

[41] J. Martin, H. Motohashi and T. Suyama, *Ultra Slow-Roll Inflation and the non-Gaussianity Consistency Relation*, *Phys. Rev. D* **87** (2013) 023514 [`arXiv:1211.0083`] [ɪɴSPIRE].

[42] Y.-F. Cai et al., *Revisiting non-Gaussianity from non-attractor inflation models*, *JCAP* **05** (2018) 012 [`arXiv:1712.09998`] [ɪɴSPIRE].

[43] J.S. Bullock and J.R. Primack, *NonGaussian fluctuations and primordial black holes from inflation*, *Phys. Rev. D* **55** (1997) 7423 [`astro-ph/9611106`] [ɪɴSPIRE].

[44] P. Ivanov, *Nonlinear metric perturbations and production of primordial black holes*, *Phys. Rev. D* **57** (1998) 7145 [`astro-ph/9708224`] [ɪɴSPIRE].

[45] J. Yokoyama, *Chaotic new inflation and formation of primordial black holes*, *Phys. Rev. D* **58** (1998) 083510 [`astro-ph/9802357`] [ɪɴSPIRE].

[46] C.T. Byrnes, E.J. Copeland and A.M. Green, *Primordial black holes as a tool for constraining non-Gaussianity*, *Phys. Rev. D* **86** (2012) 043512 [`arXiv:1206.4188`] [ɪɴSPIRE].

[47] E.V. Bugaev and P.A. Klimai, *Primordial black hole constraints for curvaton models with predicted large non-Gaussianity*, *Int. J. Mod. Phys. D* **22** (2013) 1350034 [`arXiv:1303.3146`] [ɪɴSPIRE].

[48] S. Young and C.T. Byrnes, *Primordial black holes in non-Gaussian regimes*, *JCAP* **08** (2013) 052 [`arXiv:1307.4995`] [ɪɴSPIRE].

[49] S. Young, D. Regan and C.T. Byrnes, *Influence of large local and non-local bispectra on primordial black hole abundance*, *JCAP* **02** (2016) 029 [`arXiv:1512.07224`] [ɪɴSPIRE].

[50] G. Franciolini, A. Kehagias, S. Matarrese and A. Riotto, *Primordial Black Holes from Inflation and non-Gaussianity*, *JCAP* **03** (2018) 016 [arXiv:1801.09415] [INSPIRE].

[51] M. Biagetti, G. Franciolini, A. Kehagias and A. Riotto, *Primordial Black Holes from Inflation and Quantum Diffusion*, *JCAP* **07** (2018) 032 [arXiv:1804.07124] [INSPIRE].

[52] V. Atal and C. Germani, *The role of non-gaussianities in Primordial Black Hole formation*, *Phys. Dark Univ.* **24** (2019) 100275 [arXiv:1811.07857] [INSPIRE].

[53] S. Passaglia, W. Hu and H. Motohashi, *Primordial black holes and local non-Gaussianity in canonical inflation*, *Phys. Rev. D* **99** (2019) 043536 [arXiv:1812.08243] [INSPIRE].

[54] V. De Luca et al., *The Ineludible non-Gaussianity of the Primordial Black Hole Abundance*, *JCAP* **07** (2019) 048 [arXiv:1904.00970] [INSPIRE].

[55] M. Taoso and A. Urbano, *Non-gaussianities for primordial black hole formation*, *JCAP* **08** (2021) 016 [arXiv:2102.03610] [INSPIRE].

[56] M.W. Davies, P. Carrilho and D.J. Mulryne, *Non-Gaussianity in inflationary scenarios for primordial black holes*, *JCAP* **06** (2022) 019 [arXiv:2110.08189] [INSPIRE].

[57] V. De Luca and A. Riotto, *A note on the abundance of primordial black holes: Use and misuse of the metric curvature perturbation*, *Phys. Lett. B* **828** (2022) 137035 [arXiv:2201.09008] [INSPIRE].

[58] T. Matsubara and M. Sasaki, *Non-Gaussianity effects on the primordial black hole abundance for sharply-peaked primordial spectrum*, *JCAP* **10** (2022) 094 [arXiv:2208.02941] [INSPIRE].

[59] D.S. Salopek and J.R. Bond, *Nonlinear evolution of long wavelength metric fluctuations in inflationary models*, *Phys. Rev. D* **42** (1990) 3936 [INSPIRE].

[60] M. Sasaki and E.D. Stewart, *A General analytic formula for the spectral index of the density perturbations produced during inflation*, *Prog. Theor. Phys.* **95** (1996) 71 [astro-ph/9507001] [INSPIRE].

[61] A.A. Starobinsky, *Multicomponent de Sitter (Inflationary) Stages and the Generation of Perturbations*, *JETP Lett.* **42** (1985) 152 [INSPIRE].

[62] M. Sasaki and T. Tanaka, *Superhorizon scale dynamics of multiscalar inflation*, *Prog. Theor. Phys.* **99** (1998) 763 [gr-qc/9801017] [INSPIRE].

[63] D.H. Lyth, K.A. Malik and M. Sasaki, *A General proof of the conservation of the curvature perturbation*, *JCAP* **05** (2005) 004 [astro-ph/0411220] [INSPIRE].

[64] H.-C. Lee et al., *A New delta N formalism for multi-component inflation*, *JCAP* **10** (2005) 004 [astro-ph/0506262] [INSPIRE].

[65] D.H. Lyth and Y. Rodriguez, *The Inflationary prediction for primordial non-Gaussianity*, *Phys. Rev. Lett.* **95** (2005) 121302 [astro-ph/0504045] [INSPIRE].

[66] A.A. Abolhasani, H. Firouzjahi, A. Naruko and M. Sasaki, *Delta N Formalism in Cosmological Perturbation Theory*, WSP (2019) [DOI:10.1142/10953] [INSPIRE].

[67] V. Atal, J. Garriga and A. Marcos-Caballero, *Primordial black hole formation with non-Gaussian curvature perturbations*, *JCAP* **09** (2019) 073 [arXiv:1905.13202] [INSPIRE].

[68] V. Atal, J. Cid, A. Escrivà and J. Garriga, *PBH in single field inflation: the effect of shape dispersion and non-Gaussianities*, *JCAP* **05** (2020) 022 [arXiv:1908.11357] [INSPIRE].

[69] M. Biagetti et al., *The formation probability of primordial black holes*, *Phys. Lett. B* **820** (2021) 136602 [arXiv:2105.07810] [INSPIRE].

[70] N. Kitajima, Y. Tada, S. Yokoyama and C.-M. Yoo, *Primordial black holes in peak theory with a non-Gaussian tail*, *JCAP* **10** (2021) 053 [arXiv:2109.00791] [INSPIRE].

[71] A.D. Gow et al., *Non-perturbative non-Gaussianity and primordial black holes*, *EPL* **142** (2023) 49001 [arXiv:2211.08348] [INSPIRE].

[72] G. Ferrante, G. Franciolini, J.A. Iovino and A. Urbano, *Primordial non-Gaussianity up to all orders: Theoretical aspects and implications for primordial black hole models*, *Phys. Rev. D* **107** (2023) 043520 [arXiv:2211.01728] [INSPIRE].

[73] S. Pi and M. Sasaki, *Logarithmic Duality of the Curvature Perturbation*, *Phys. Rev. Lett.* **131** (2023) 011002 [arXiv:2211.13932] [INSPIRE].

[74] C. Pattison, V. Vennin, H. Assadullahi and D. Wands, *Quantum diffusion during inflation and primordial black holes*, *JCAP* **10** (2017) 046 [arXiv:1707.00537] [INSPIRE].

[75] J.M. Ezquiaga, J. García-Bellido and V. Vennin, *The exponential tail of inflationary fluctuations: consequences for primordial black holes*, *JCAP* **03** (2020) 029 [arXiv:1912.05399] [INSPIRE].

[76] D.G. Figueroa, S. Raatikainen, S. Rasanen and E. Tomberg, *Non-Gaussian Tail of the Curvature Perturbation in Stochastic Ultraslow-Roll Inflation: Implications for Primordial Black Hole Production*, *Phys. Rev. Lett.* **127** (2021) 101302 [arXiv:2012.06551] [INSPIRE].

[77] C. Pattison, V. Vennin, D. Wands and H. Assadullahi, *Ultra-slow-roll inflation with quantum diffusion*, *JCAP* **04** (2021) 080 [arXiv:2101.05741] [INSPIRE].

[78] N. Ahmadi et al., *Quantum diffusion in sharp transition to non-slow-roll phase*, *JCAP* **08** (2022) 078 [arXiv:2207.10578] [INSPIRE].

[79] C. Animali and V. Vennin, *Primordial black holes from stochastic tunnelling*, *JCAP* **02** (2023) 043 [arXiv:2210.03812] [INSPIRE].

[80] K. Inomata, E. McDonough and W. Hu, *Amplification of primordial perturbations from the rise or fall of the inflaton*, *JCAP* **02** (2022) 031 [arXiv:2110.14641] [INSPIRE].

[81] Y.-F. Cai et al., *One small step for an inflaton, one giant leap for inflation: A novel non-Gaussian tail and primordial black holes*, *Phys. Lett. B* **834** (2022) 137461 [arXiv:2112.13836] [INSPIRE].

[82] Y.-F. Cai et al., *Highly non-Gaussian tails and primordial black holes from single-field inflation*, *JCAP* **12** (2022) 034 [arXiv:2207.11910] [INSPIRE].

[83] A. Gallego Cadavid and A.E. Romano, *Effects of discontinuities of the derivatives of the inflaton potential*, *Eur. Phys. J. C* **75** (2015) 589 [arXiv:1404.2985] [INSPIRE].

[84] S.S. Mishra and V. Sahni, *Primordial Black Holes from a tiny bump/dip in the Inflaton potential*, *JCAP* **04** (2020) 007 [arXiv:1911.00057] [INSPIRE].

[85] K. Kefala, G.P. Kodaxis, I.D. Stamou and N. Tetradis, *Features of the inflaton potential and the power spectrum of cosmological perturbations*, *Phys. Rev. D* **104** (2021) 023506 [arXiv:2010.12483] [INSPIRE].

[86] K. Inomata, E. McDonough and W. Hu, *Primordial black holes arise when the inflaton falls*, *Phys. Rev. D* **104** (2021) 123553 [arXiv:2104.03972] [INSPIRE].

[87] I. Dalianis et al., *Spectrum oscillations from features in the potential of single-field inflation*, *Phys. Rev. D* **104** (2021) 103510 [arXiv:2106.02467] [INSPIRE].

[88] R. Zheng, J. Shi and T. Qiu, *On primordial black holes and secondary gravitational waves generated from inflation with solo/multi-bumpy potential*, *Chin. Phys. C* **46** (2022) 045103 [arXiv:2106.04303] [INSPIRE].

[89] R. Kawaguchi and S. Tsujikawa, *Primordial black holes from Higgs inflation with a Gauss-Bonnet coupling*, *Phys. Rev. D* **107** (2023) 063508 [`arXiv:2211.13364`] [ɪɴSPIRE].

[90] B.-M. Gu, F.-W. Shu, K. Yang and Y.-P. Zhang, *Primordial black holes from an inflationary potential valley*, *Phys. Rev. D* **107** (2023) 023519 [`arXiv:2207.09968`] [ɪɴSPIRE].

[91] C. Fu and S.-J. Wang, *Primordial black holes and induced gravitational waves from double-pole inflation*, *JCAP* **06** (2023) 012 [`arXiv:2211.03523`] [ɪɴSPIRE].

[92] Y. Cai, M. Zhu and Y.-S. Piao, *Primordial black holes from null energy condition violation during inflation*, `arXiv:2305.10933` [ɪɴSPIRE].

[93] J. Kristiano and J. Yokoyama, *Ruling Out Primordial Black Hole Formation From Single-Field Inflation*, `arXiv:2211.03395` [ɪɴSPIRE].

[94] K. Inomata, M. Braglia, X. Chen and S. Renaux-Petel, *Questions on calculation of primordial power spectrum with large spikes: the resonance model case*, *JCAP* **04** (2023) 011 [`arXiv:2211.02586`] [ɪɴSPIRE].

[95] S. Choudhury, M.R. Gangopadhyay and M. Sami, *No-go for the formation of heavy mass Primordial Black Holes in Single Field Inflation*, `arXiv:2301.10000` [ɪɴSPIRE].

[96] S. Choudhury, S. Panda and M. Sami, *PBH formation in EFT of single field inflation with sharp transition*, *Phys. Lett. B* **845** (2023) 138123 [`arXiv:2302.05655`] [ɪɴSPIRE].

[97] S. Choudhury, S. Panda and M. Sami, *Quantum loop effects on the power spectrum and constraints on primordial black holes*, `arXiv:2303.06066` [ɪɴSPIRE].

[98] J. Kristiano and J. Yokoyama, *Response to criticism on "Ruling Out Primordial Black Hole Formation From Single-Field Inflation": A note on bispectrum and one-loop correction in single-field inflation with primordial black hole formation*, `arXiv:2303.00341` [ɪɴSPIRE].

[99] H. Firouzjahi, *One-loop Corrections in Power Spectrum in Single Field Inflation*, `arXiv:2303.12025` [ɪɴSPIRE].

[100] A. Riotto, *The Primordial Black Hole Formation from Single-Field Inflation is Not Ruled Out*, `arXiv:2301.00599` [ɪɴSPIRE].

[101] A. Riotto, *The Primordial Black Hole Formation from Single-Field Inflation is Still Not Ruled Out*, `arXiv:2303.01727` [ɪɴSPIRE].

[102] H. Firouzjahi and A. Riotto, *Primordial Black Holes and Loops in Single-Field Inflation*, `arXiv:2304.07801` [ɪɴSPIRE].

[103] G. Franciolini, J.A. Iovino, M. Taoso and A. Urbano, *One loop to rule them all: Perturbativity in the presence of ultra slow-roll dynamics*, `arXiv:2305.03491` [ɪɴSPIRE].

[104] G. Tasinato, *Large $|\eta|$ approach to single field inflation*, *Phys. Rev. D* **108** (2023) 043526 [`arXiv:2305.11568`] [ɪɴSPIRE].

[105] H. Motohashi and Y. Tada, *Squeezed bispectrum and one-loop corrections in transient constant-roll inflation*, `arXiv:2303.16035` [ɪɴSPIRE].

[106] S. Choudhury, S. Panda and M. Sami, *Galileon inflation evades the no-go for PBH formation in the single-field framework*, `arXiv:2304.04065` [ɪɴSPIRE].

[107] X. Chen, R. Easther and E.A. Lim, *Generation and Characterization of Large Non-Gaussianities in Single Field Inflation*, *JCAP* **04** (2008) 010 [`arXiv:0801.3295`] [ɪɴSPIRE].

[108] C.T. Byrnes, P.S. Cole and S.P. Patil, *Steepest growth of the power spectrum and primordial black holes*, *JCAP* **06** (2019) 028 [`arXiv:1811.11158`] [ɪɴSPIRE].